BENZOXAZOLE AND BENZOTHIAZOLE DERIVATIVES AS POTENTIAL FLUORESCENCE IMAGING AGENTS

A THESIS
SUBMITTED TO THE FACULTY OF THE GRADUATE SCHOOL
OF THE UNIVERSITY OF MINNESOTA
BY

SARAH GEPPERT

IN PARTIAL FULFILLMENT OF THE REQUIREMENTS
FOR THE DEGREE OF
MASTER OF SCIENCE

Dr. Paul Kiprof

August, 2019

Acknowledgements

I would like to give a special thanks to my advisor, Dr. Paul Kiprof, for his help and encouragement throughout my time as his graduate student. I would also like to thank Dr. Ahmed Heikal for his expertise and equipment without which this project would not have been possible. Thank you to Dr. Benjamin Clarke for being a member of my graduate committee and for his willingness to help me explore the possibilities within my research project. Thank you to Dr. Venkatram Mereddy for serving on my committee and being a gracious teacher and nearest (lab) neighbor. Thank you also to W.P.M. Dhanushka Wickramasinghe for all her assistance.

I would also like to acknowledge the work of Christian Toonstra, Jeffery Carlson, Aaron Skoglund, Shannon Redbrook, Peggy Walsh, Randi Timerman and Peter Steltz.

Dedication

This project is dedicated to my father, the late Gary Geppert and my late mother, Kay Geppert. Without them I would never have pursued science.

Abstract: Substituted Benzoxazole (1-hydroxy-2-naphthoic benzoxazole and 2-hydroxy-3-naphthoic benzoxazole) and benzothiazole (1-hydroxy-2-naphthoic benzoxazole and 2-hydroxy-3-naphthoic benzothiazole) derivatives previously complexed with Boron-containing fragments in our lab, were reviewed for potential use in Fluorescence Lifetime Imaging Microscopy (FLIM) with Differential Interference Contrast (DIC) microscopy in adherent cells. The Excited State Intramolecular Proton Transfer (ESIPT), excited state tautomerization, and potential chelating properties inherent to these compounds prompted our research. The flexible nature of the molecules in two key bonds, when compared to that of other fluorophores, contributed to an inherent quantum inefficiency resulting in reduced brightness when compared to commercially available fluorescent dyes like fluorescein. The quantum chemical study of the photochemistry and conformational preference of these compounds was not able to accurately predict absorbance characteristics, but provided insight into the ESIPT process and established a strong conformational preference for one conformer. The unique properties of these ligands and similar compounds may still be of biophotochemical interest and warrant further investigation.

Table of Contents

List of Tables

List of Schemes

List of Figures

Abbreviations List

AD – Alzheimer's Disease

BM –2-(2-aminophyenyl)-1*H* benzimidazole

DIC – Differential Interference Contrast (microscopy)

ESIPT – Excited State Intramolecular Proton Transfer

FCS – Fluorescence Correlation Spectroscopy

FLIM – Fluorescence Lifetime Imaging Microscopy

FRAP – Fluorescence Recovery After Photobleaching

FRET – Förster Resonance Energy Transfer

HBO – 2-(2-hydroxyphenyl) benzoxazole

HBT –2-(2-hydroxyphenyl) benzothiazole

12HNBO – 1-hydroxy-2-naphthoic benzoxazole

12HNBT – 1-hydroxy-2-naphthoic benzothiazole

23HNBO – 2-hydroxy-3-naphthoic benzoxazole

23HNBT – 2-hydroxy-3-naphthoic benzothiazole

DCM – Dichloromethane

DMSO – Dimethyl Sulfoxide

1. Introduction and Background

Fluorescence Microscopy has become a cutting-edge tool in medical and biochemical research. The name "fluorescence microscopy" encompasses a large variety of techniques such as Fluorescence Correlation Spectroscopy (FCS), Fluorescence Recovery After Photobleaching (FRAP), Förster Resonance Energy Transfer (FRET), and Fluorescence Lifetime Imaging Microscopy (FLIM). [1] These techniques allow the scientist to investigate biological systems and biochemical pathways using the auto-fluorescence of the system or through a fluorescent probe or dye that is inserted into the biological system, respectively.

Fluorescent dyes are used for a variety of purposes in biological studies. Probes may be attached to a component of the system—such as proteins or nucleic acids—to track it in real time. Some dyes are taken up into cells to specific areas in the cell or only when the cell is unhealthy and may thus be used for co-localization studies or viability assays respectively. [2] Our lab has recently used fluorescent benzoxazole and benzothiazole derivatives as dyes in light-emitting applications. [3–5]

1.1 Fluorescence

Fluorescence was observed as early as the 16th century, but the first to scientifically describe the phenomenon was John Herschal in 1845.[6,7] It was George Stokes a few years later that first termed it "fluorescence".[8] Fluorescence occurs when a molecule is able to absorb enough energy for an electron to move to a higher energy orbital, placing the molecule from the ground state to an excited state but rather than

returning to the ground state through dissipating energy through non-radiative processes, the molecule releases excess energy as light. The light emitted is always at a longer wavelength from which it was excited because of Internal Conversion that places the molecule in a lower vibrational state, additionally the emission of light is typically to an excited vibrational level of the electronic ground state, both radiationless processes lower the energy of the emitted photon compared to the absorbed photon slightly; the difference between the two is called the Stokes shift. The timeframe for this event is on the order of nanoseconds. Fluorescence is distinct from the other form of luminescence, phosphorescence.

Phosphorescence occurs when there is a transition (Intersystem Crossing) from the excited state to a different spin-state, typically a triplet state for organic molecules but since it is "forbidden" in quantum mechanics to go from a triplet state to ground state, light emission is much slower than that of fluorescence. [9] Both processes are useful in biomedical diagnostic techniques as well as materials applications. They have in common that they are photoluminescent processes that emit light after light is being absorbed. Some of the same compounds that are exhibiting photoluminescence also are suitable for electroluminescence such as in OLED applications[10–12]

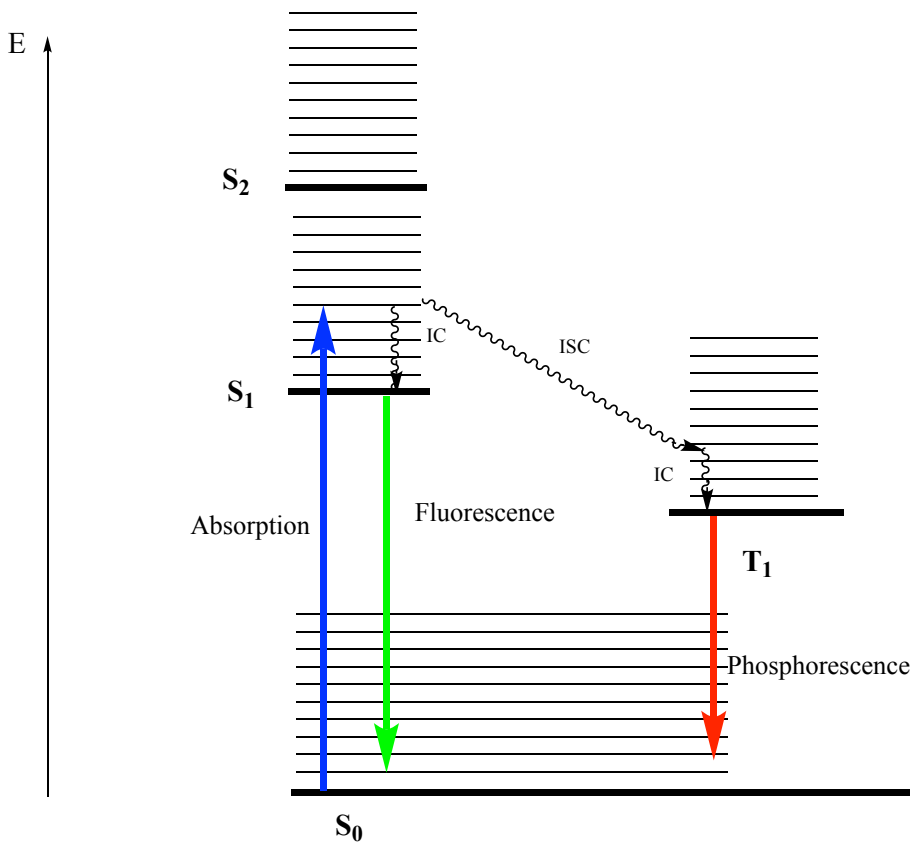

Figure 1: Jablonski diagram comparing fluorescence and phosphorescence showing the electronic ground and excited states.

There are two general approaches to measuring photoluminescence as there are two changeable energy parameters. The input wavelength and the observed wavelength can be varied. An excitation spectrum is measured through varying the input wavelength while observing a constant wavelength known to emit. Emission spectra are normally measured using a specific wavelength of excitation and varying the detection of the output wavelength. Zero order excitation or emission spectra are measured using the fluorescence signal at all wavelengths. Thus, it is common to identify all of the peaks of

an emission spectrum for a new compound and find the corresponding excitation wavelengths.[1]

In rigid molecules the absorption wavelength is identical or very nearly identical to the excitation wavelength of the molecule. Because of the rigidity of a molecule, energy cannot be dissipated in radiationless processes (Internal Conversion) and the geometry of the molecule in the excited state ends up close to the geometry in the ground state. The excitation and emission spectra are measured using a spectrofluorometer (or fluorometer for short). Rigid fluorophores undergo minimum conformational rotation and generally have an absorbance spectrum very similar to the excitation spectrum. In contrast, flexible molecules may undergo a significant conformational change from a ground state to an excited state such that antibonding, or nonbonding, molecular orbitals are populated. This can change the bonding within the fluorophore, causing a large Stokes shift.

In particular, there is a class of molecules that undergo an Excited-State Intramolecular Proton Transfer, or ESIPT.[13–22] This occurs when previously unoccupied molecular orbitals are populated in the excited state changing the charge distribution in the molecule and the proton shifts to a more negatively charged atom, creating a tautomeric form of the molecule. Kasha and coworkers studied this phenomenon now termed ESIPT [21] and it has been observed, solvent-assisted, non-solvent assisted and in intermolecular variations.[22]

For example, the molecules discussed in this paper can undergo ESIPT due to the proximity of the hydroxyl group to a basic nitrogen atom. The hydroxyl group becomes

more acidic while the aromatic amine becomes more basic in the excited state, after the light absorption process. The proton transfer then occurs and the molecule exists in its tautomeric form in an excited state that is slightly lower in energy because of the geometry change. Thus, the emission of light happens from the tautomeric form leading to a large Stokes shift. After the emission of light there is a reverse proton transfer as the charge distribution is now closer to the ground state and the molecule in its original ground state is re-formed. This is a well-documented phenomenon for hydrophenyl- and hydroxynaphtyl-substituted azoles (Figure 2). [23,24]

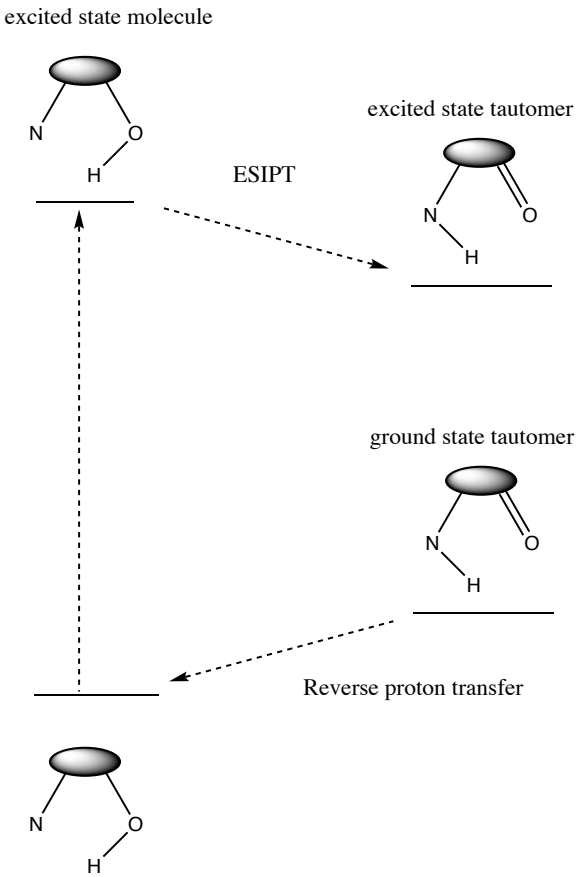

Figure 2: The basic scheme for an Excited State Intramolecular Proton Transfer (ESIPT) in a molecule containing a hydroxyl group and a nitrogen with a lone pair of electrons.

The Stokes shift can also be affected by the nature of the solvent environment surrounding the fluorophore. Polar and non-polar solvents can result in bathochromic or hypsochromic shifts in the spectra. This is primarily important for polar fluorophores.

Quenching, when referring to fluorescence, describes any number of processes that decrease the intensity of fluorescence and dissipate energy by bypassing light emission. Common types of quenching studied are collisional quenching, static quenching, and self-quenching. Collisional quenching occurs when a fluorescent molecule collides with quenching molecule resulting in a non-fluorescent transfer in energy. Collisional quenching can be modeled by the Stern-Volmer equation. Static quenching results when a fluorophore forms a complex with the quenching molecule while still in the ground state and therefore does not fluoresce upon excitation. Static quenching is not dependent on diffusion or collisions. [1] Self-quenching refers to the phenomenon where fluorescence intensity no longer increases with concentration because the fluorophore is colliding with itself.

1.2 Fluorescence Lifetime Imaging Microscopy (FLIM) and Differential Interference Contrast (DIC) Microscopy

When fluorescent molecules relax from an excited state to a ground state, photons are emitted. However, the time required for this to occur is dependent on several factors—most importantly the polarity of the environment. FLIM results are divided into two parts: the intensity image, and the lifetime image. The intensity image is a black and

white representation of the intensity of the fluorescence per pixel. The lifetime image is a color-coded representation of the fluorescence lifetime ranging from blue to red. [7]

Differential Interference Contrast (DIC) microscopy is a research technique in light microscopy that allows the investigator to view a microscopic object with significant clarity. Using a series of specialized prisms and lenses, light is polarized, separated into two signals, and passed through a condenser lens, the sample, an objective lens and then finally recombined. The difference in the phase shift of the light displays interference contrast, allowing the user to view the microscopic object. [25–27]

1.3 Previous Research with hydroxyphenyl azoles

Substituted azoles, such as found in Figure 2, have been studied extensively in the past for their Excited-State Intramolecular Proton Transfer properties. Kleinschmidt and Graness published several papers beginning in 1983. [28] Since then, numerous papers have been published, investigating the ESIPT characteristics not only as a means to understand the phenomenon alone, but also to better understand the photochromism of salicylidene anilines, which undergo a complex structural rearrangement in the excited state. [24,23]

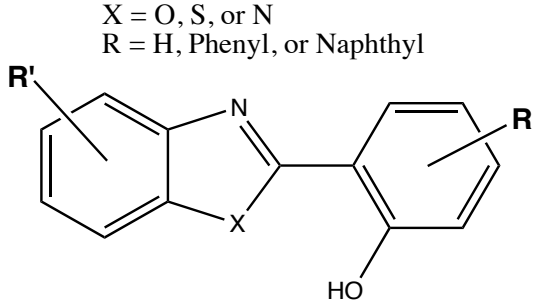

Figure 3: Substituted azoles previously studied for fluorescence and Excited State Intramolecular Proton Transfer.

1-hydroxy-2-napthoicbenzothiazole and 2-hydroxy-3-naphthoic benzothiazole (among other compounds) were studied as potential fluorescent probes for use in Enzyme-Linked Immunoassays (ELISA). Molecules were selected to be initially non-fluorescent and water soluble prior to assay, and subsequently convertible via enzymatic reaction with an antibody into insoluble fluorophores with the hope of creating an instant type test similar to that of pregnancy tests and diaper indicators.[51]

In 2001, Tanaka et al investigated various fluorinated derivatives of 2-(2-hydroxyphenyl)benzoxazole and 2-(2-hydroxyphenyl)benzothiazole for the purpose of selecting fluorescent probes sensitive to pH and metal cations. The investigators were particularly interested in utilizing the intramolecular proton transfer and subsequent dual emission characteristics as a means of detecting metallic cation concentrations or pH with high sensitivity.[29]

In 2009, Rodriguez-Rodriguez et al. published a paper regarding the use of compounds similar to ours as potential fluorescent dyes for use in Alzheimer's research and possibly treatment. The study noted that thioflavin-T (along with Congo red) has reliably been used to image β-amyloid plaques in vitro. Clioquinol has undergone animal trials in metal chelation therapy for Alzheimer's disease (AD). Thus, combining the general structure of thioflavin T with the chelation site of clioquinol, they examined three different compounds: 2-(2-hydroxyphenyl) benzoxazole (HBO), 2-(2-hydroxyphenyl) benzothiazole (HBT), and 2-(2-aminophyenyl)-1*H* benzimidizole (BM). [30]

One of the experimental goals of the paper was to determine whether or not these readily available compounds could be shown to intercalate into the β-sheet structure of β-

amyloid plaques and be imaged using fluorescence. The results showed no perceivable activity with HBO, or BM but some response from HBT.

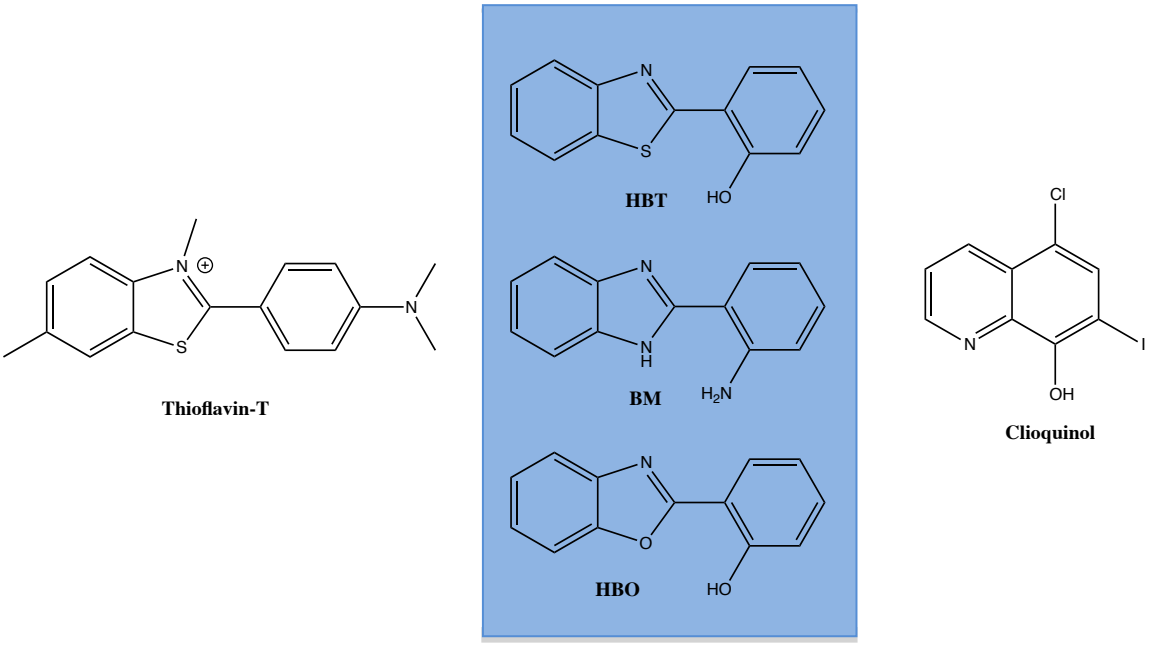

Figure 4: Comparison of Thioflavin-T and Clioquinol with HBT, BM, and HBO

A 2009 study proposed the middle three molecules for study, hoping to combine the chelating properties of Cliquinol and the fluorescent dye properties of Thioflavin-T. [30]

Substituted azoles have also been studied when chelated. Boron-azole complexes are especially luminescent and have been investigated for potential use in Organic Light Emitting Diode devices. [31–34] Medicinal value for metal chelated hydroxylnaphtyl-substituted benzoxazoles has also been investigated for antimicrobial activity. The

magnesium complex and the nickel complexes were shown to have significant anti-fungal properties against two of the four tested fungal cultures. [35]

Chapter II: Experimental Methods

2.1 Synthesis and Purification of the Compounds

All synthesis and purification were done according to the schemes specified by our lab's previous research. [5]

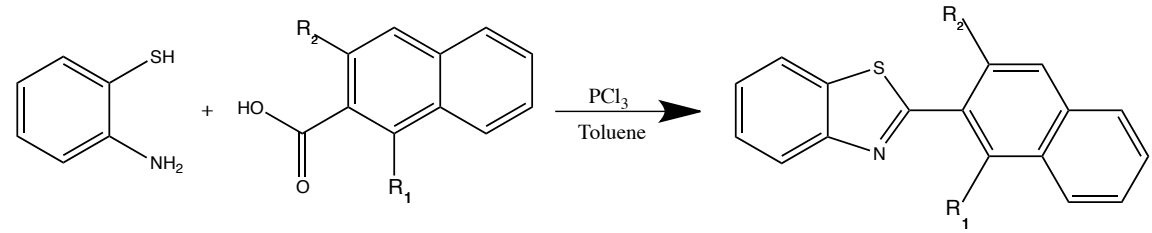

2-aminothiophenol

1-hydroxy-2-naphthoic acid
2-hydroxy-3-naphthoic acid

12HNBT $R_1 = OH$ $R_2 = H$
23HNBT $R_1 = H$ $R_2 = OH$

Scheme 1: Synthesis of substituted Hydroxynapthanoic benzothiazoles**.**

12HNBT (1-hydroxy-2-naphthoicbenzthiazole)

In a 50-150 mL two-neck round bottom flask, toluene (21 mL) brought to a boil. Upon boiling, 1-hydroxy-2-naphthoic acid (2.77g, 10 mmol) and 2-aminothiophenol (1.39 g, 11 mmol) is added to the flask. Upon dissolution of the reactants, a heterogeneous mixture occurs and the vessel is then allowed to cool to 90°C. Upon cooling, a PCl_3 (1.37g, 10 mmol) and toluene (5 mL) mixture is very carefully added dropwise (or the reaction will be too vigorous and likely overflow). After all of the PCl_3 solution was added, the mixture was allowed to reflux for 2 hours and then cooled to

60°C. The product was precipitated using cold methanol (40 mL). The precipitate was filtered, washed with additional cold methanol and then recrystallized with acetone.

23HNBT (2-hydroxy-3-naphthoicbenzthiazole)

The synthesis for this compound followed the same scheme as for 12HNBT (1-hydroxy-2-naphthoicbenzthiazole) with the exception of 2-hydroxy-3-naphthoic acid (2.77 g, 10 mmol) in place of 1-hydroxy-2-naphthoic acid.

12HNBO (1-hydroxy-2-naphthoic benzoxazole)

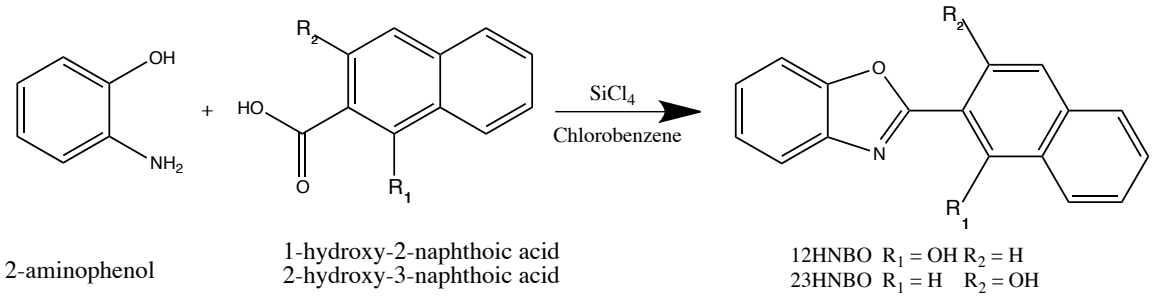

Scheme 2: Synthesis of substituted hydroxynaphthanoic benzoxazoles

In a 50-150 mL 2-arm round bottom flask, chlorobenzene (14 mL), silicon tetrachloride (1.90 g, 11mmol), and 1-hydroxy-2-naphthoic acid (2.07 g, 11 mmol) were added and a drying tube was attached to the top of a reflux condenser. The solution was heated until HCl gas was detected using litmus paper at the end of the drying tube. After the solution began to change color, 2-aminophenol (1.10 g, 10 mmol) was then added in small portions to avoid excessive reaction. The remaining solid on funnel was then rinsed with additional chlorobenzene (3 mL). The resulting mixture was then refluxed for 3

hours. To quench the reaction, a solution of saturated aqueous $NaHCO_3$ was added until the solution was basic. The chlorobenzene solvent was evaporated off using vacuum distillation. The resulting solid was then extracted with warm dichloromethane (3 x 100 mL) and filtered. The dichloromethane solution was then dried over $MgSO_4$ and concentrated using vacuum distillation. The crude product was purified using silica gel chromatography (19:1 hexanes: ethyl acetate). The final product was further purified via recrystalization with acetone.

23HNBO (2-hydroxy-3-naphthoic benzoxazole)

2-hydroxy-3-naphthoic benzoxazole was synthesized in the same manner as 12HNBO except with 2-hydroxy-3-naphthoic acid instead of 1-hydroxy-2-naphthoic acid. The product was purified in the same manner.

2.2 Experimental Spectra

Absorbance Spectra were taken on a UV-Vis Spectrophotometer. Fluorescence spectra were gathered using a Cary spectrofluorometer. Spectrophotometric grade solvents were used in all experiments. Quartz cuvettes were used on both types of machines: 2-sided on the UV-Vis spectrophotometer and 4-sided polished cuvettes on the fluorometer.

2.3 FLIM: Fluorescence Lifetime Imaging Microscopy & DIC: Differential Interference Contrast

Cell Preparation

C3H10T1/2 Cells were kept in an incubator and cared for according to standard protocols for adherent cells. In preparation for the experiment, the cell line was split and cells were deposited into a small petri dish with a well at the center specifically designed for imaging. The fluorescent dye solutions were prepared from solid the very day of the experiment using 10 mL volumetric flasks and a weigh balance accurate to the .1 mg. Spectrophotometric grade Dimethyl Sulfoxide (DMSO) was used to dissolve the dye samples. Once the solid had dissolved completely, the solution was allowed to equilibrate for at least five minutes before dyeing the cells.

The cells were incubated with approximately 5 microliters of dye solution (the amount depended on the concentration of the stock solution) for 15 minutes. After the incubation period, the cell media was replaced and was washed three times with Tyrode's solution, an isotonic buffer. The cell dishes were then transported to the laser room for experimentation. The concentration of the dye in the dish during the incubation period was 5 μM for all of the experiments, except with the dye 12HNBO, which had a concentration of 2 μM in the petri dish.

Dichroic mirrors and other settings

A Prussian Blue filter was used in each experiment. Each experiment also used low pass and high pass filters to keep out wavelengths not within the range of interest.

Data Analysis

The fluorescence intensity images were analyzed using SPCimage.[36]

2.4 Computational Chemistry

All calculations were done using GAUSSIAN 09[37] and GAUSSIAN 16[38] on the computers of the Minnesota Supercomputing Institute (MSI) of the University of Minnesota.

Chapter III: Results and Discussion

3.1 1-hydroxy-2-naphthoicbenzthiazole (12HNBT)

This compound was synthesized from 2-aminothiophenol and 1-hydroxy-2-naphthoic acid according to Scheme 3.

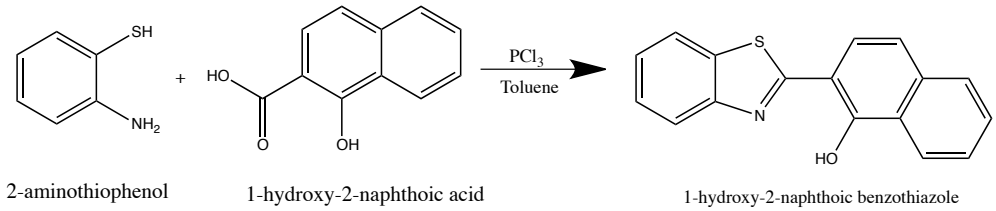

2-aminothiophenol 1-hydroxy-2-naphthoic acid 1-hydroxy-2-naphthoic benzothiazole

Scheme 3: Synthesis of 1-hydroxy-2-naphthoic benzothiazole (12HNBT)

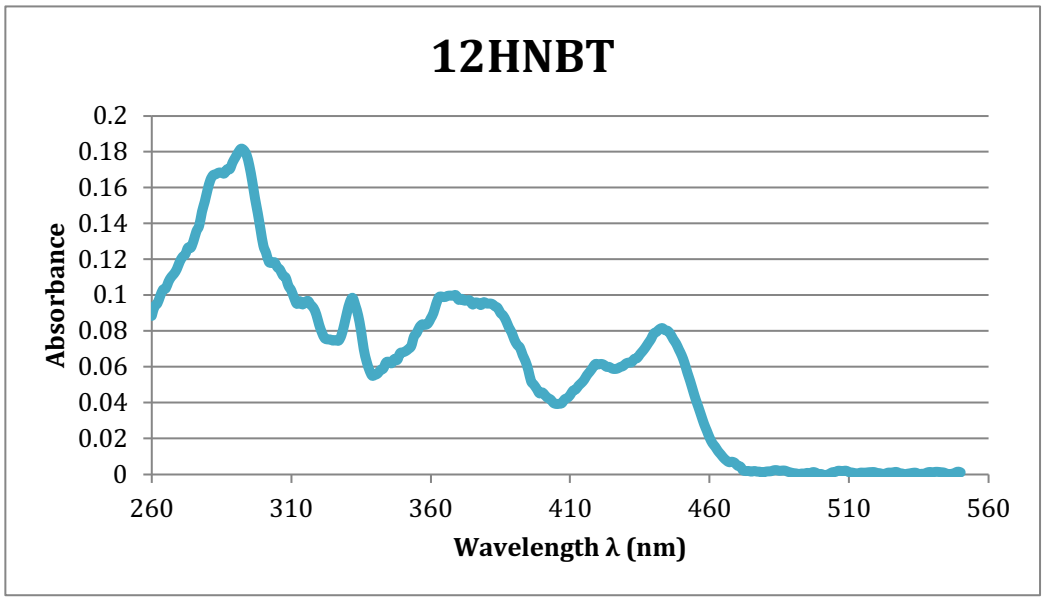

Figure 5: Absorbance spectrum of 1-hydroxy-2-naphtanoicbenzothiazole (12HNBT) in DMSO.

All spectra were taken in DMSO. The absorbance spectrum peaks (Figure 4) do not completely overlap with those of the excitation spectrum. However, the absorbance peak at 443 nm does coincide with the double peak at 437 nm and 448 nm. This was advantageous as the more red-shifted wavelength allows for a 2-photon excitation that might be impossible were the peak in the UV region.

12HNBT	Absorbance	Excitation	Emission
Wavelengths (nm)	292, 367, 380, 419, 443	392, 410	437, 448

Table 1: Absorbance, Excitation, and Emission peaks for 1-hydroxy-2-naphthoicbenzthiazole (12HNBT)

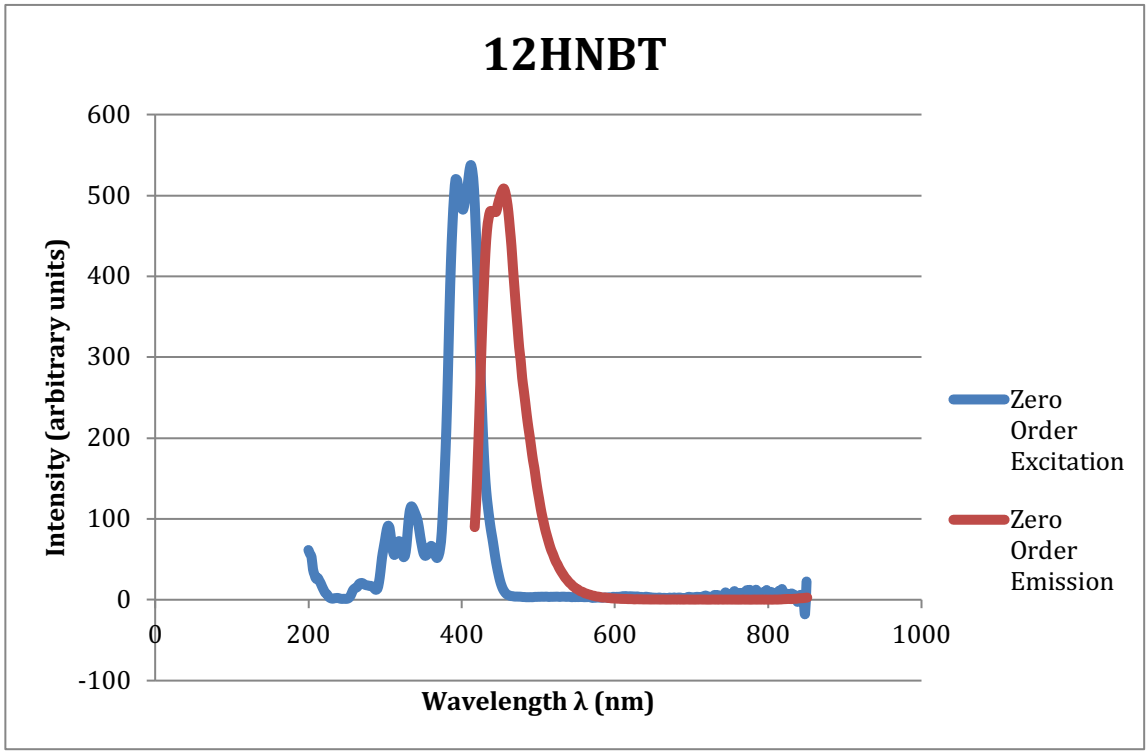

Figure 6: Zero Order Excitation and Emission spectra for 1-hydroxy-2-naphthanoicbenzothiazole in DMSO

Two-photon FLIM imaging for the compound 1-hydroxy-2-naphthoicbenzthiazole (12HNBT), the laser wavelength was set to 775 nm. A DIC image was collected before and after each FLIM image. The 2-photon wavelength was chosen based on the absorbance and excitation spectra.

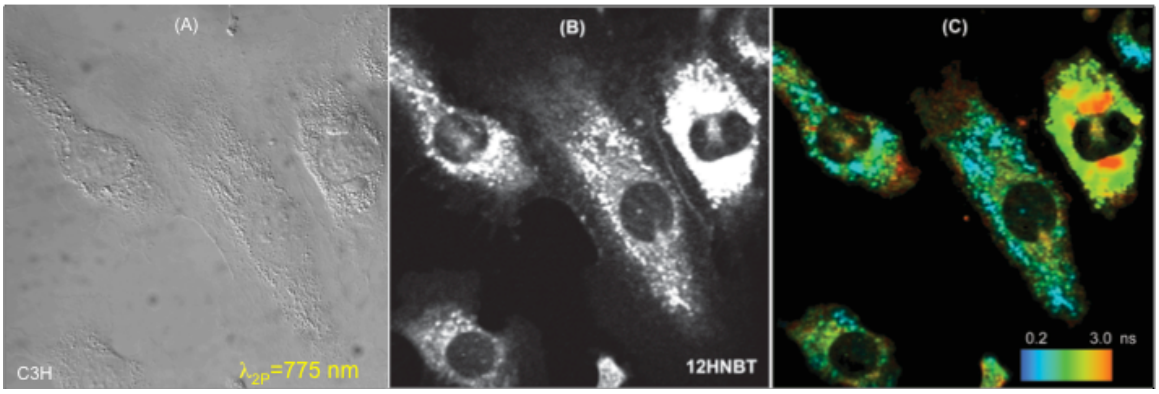

Figure 7: (A) DIC image of treated C3H cells (B) Intensity image of fluorescence signal (C) Color-coded fluorescence lifetime image of cells dyed with 1-hydroxy-2-naphthoicbenzthiazole (12HNBT)

The fluorescence lifetime decay in Figures 6 and 7 are biexponential per pixel. This suggests that there are at least two different environments within the cell that are impacting the fluorescence lifetime. In Figure 6, 48% of the fluorescence signal was found to have a lifetime of 1.3 ns and the remaining 52% a lifetime of 3.4 ns. The average lifetime was 2.2 ns. Remarkably, in two areas above and below the nucleus there is an extended fluorescence lifetime of about 3 ns. In Figure 7, the signal composition per pixel was about 70% at 660 ps and the remaining 30% at 2.6 ns. The average lifetime was

1.25 ns. In both of the figures, there is signal from within the nucleus whereas there is not in the control image. (See Appendix)

3.2 1-hydroxy-2-naphthoic benzoxazole (12HNBO)

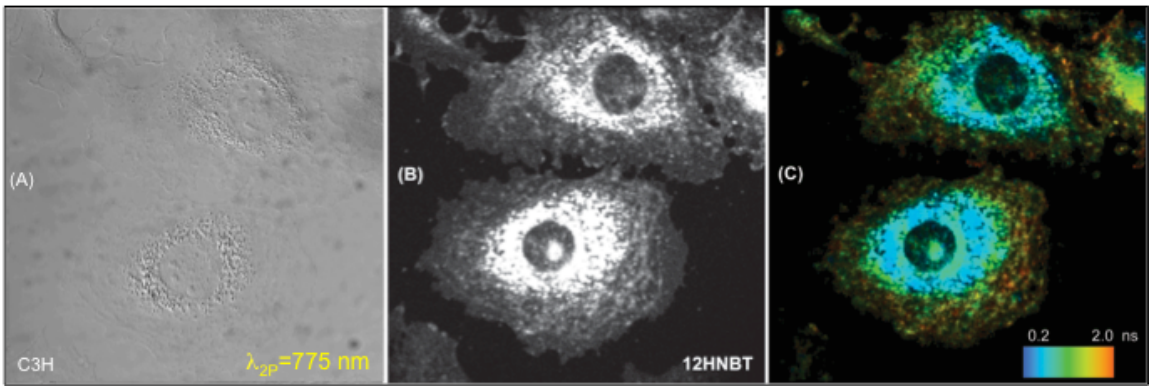

Figure 8: (A) DIC image of treated C3H cells (B) Intensity image of fluorescence signal (C) Color-coded fluorescence lifetime image of cells dyed with 1-hydroxy-2-naphthoicbenzthiazole (12HNBT)

This Compound was synthesized from 1-hydroxy-2-naphthoic acid and 2-aminophenol according to Scheme 3. The absorbance measurement was done in DMSO and showed peaks at wavelengths of 290, 370, and 415 nm.

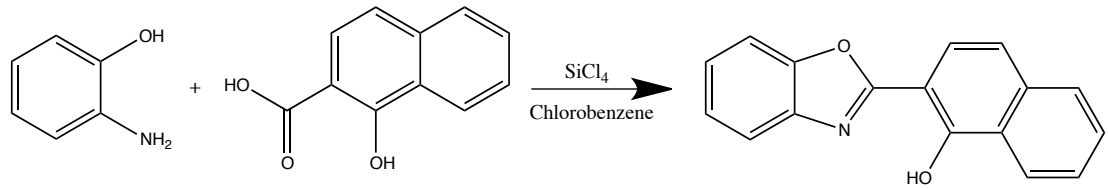

2-aminophenol 1-hydroxy-2-naphthoic acid 1-hydroxy-2-naphthoic benzoxazole

Scheme 4: Synthesis of 1-hydroxy-2-naphthoic benzoxazole (12HNBO)

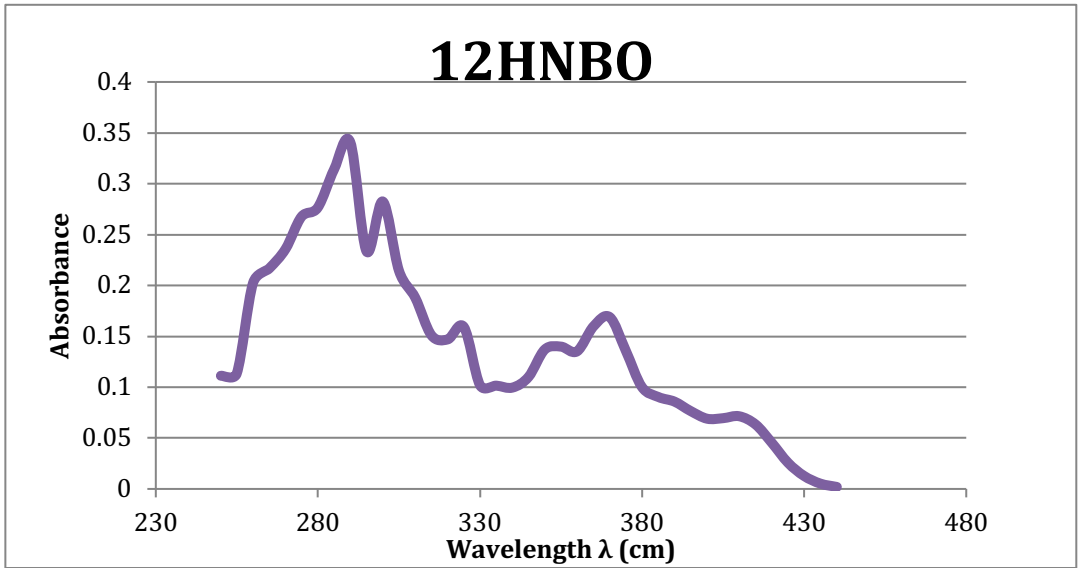

Figure 9: Absorption spectrum of 1-hydroxy 2-napthnoic benzoxazole in DMSO

These peaks did not completely overlap with the excitation spectrum shown together with the emission spectrum in Figure 9. This is likely due to the ESIPT in this compound. Excitation peaks were found at 294, 374, and 384 nm. The wavelength used for 2P-FLIM was 775 nm. The fluorescence decay lifetime is biexponential per pixel, indicating that the fluorophore encountered at least two different environments within the cell.

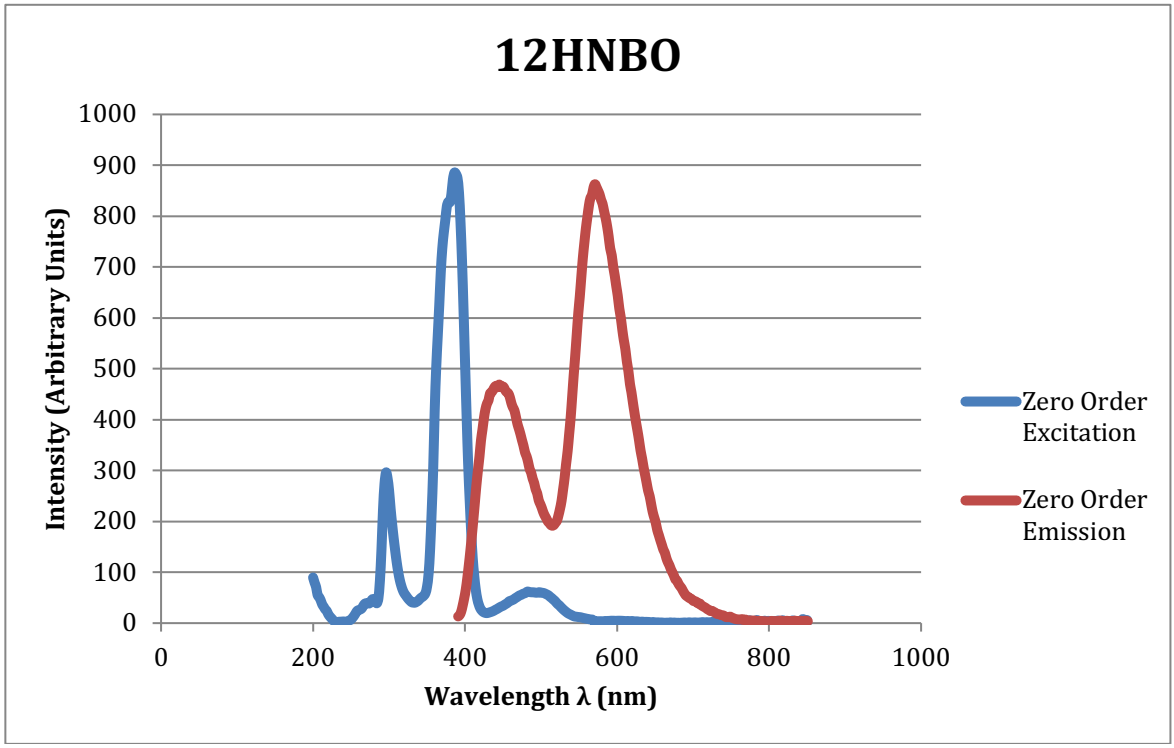

Figure 10: Zero order fluorescence excitation and emission spectra of 1-hydroxy 2-naphthnoic benzoxazole in DMSO

12HNBO	Absorbance	Excitation	Emission
Wavelengths (nm)	294, 374, 384	294, 384	428, 568

Table 2: Absorbance, Excitation, and Emission peaks for 1-hydroxy-2-naphthoic benzoxazole (12HNBO)

Approximately 75% of the lifetime decay distribution for Figure 10 occurred at 371 ps and 25% at 2.1 ns. The mean lifetime was 825 ps.

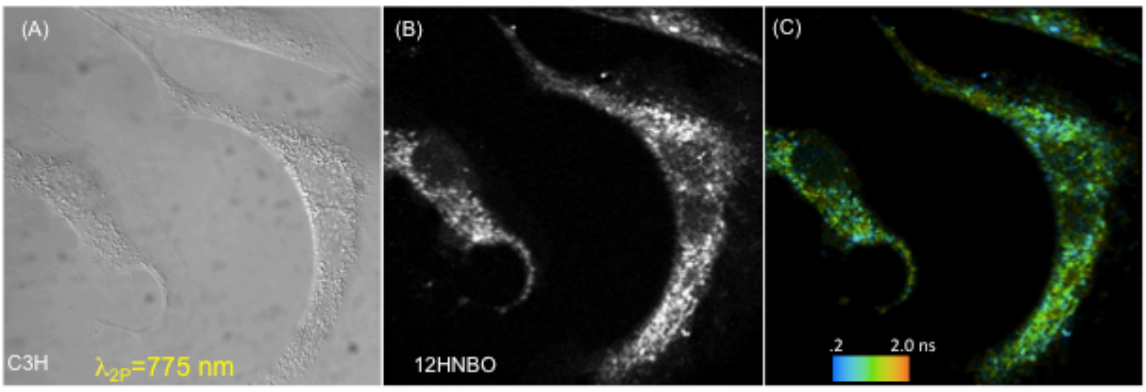

Figure 11: (A) DIC image (B) Intensity image (C) Color-coded fluorescence lifetime image of cells dyed with 12HNBO (1-hydroxy-2-naphthoic benzoxazole)

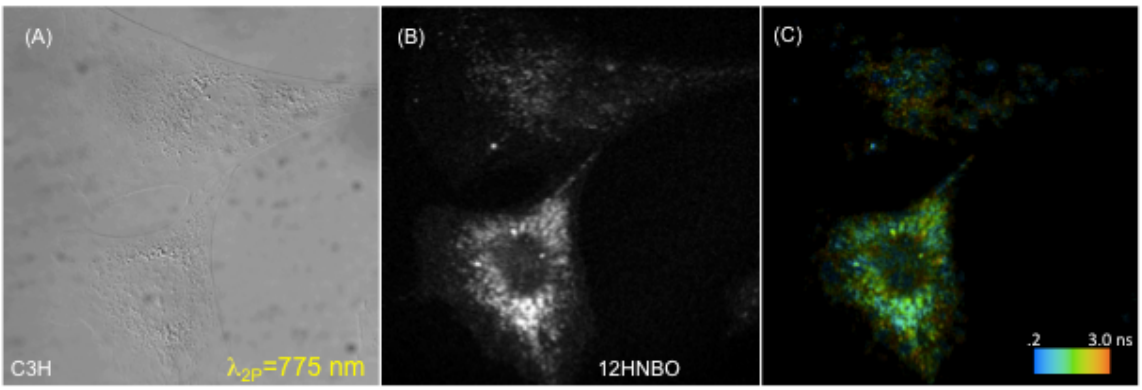

Figure 12: (A) DIC image (B) Intensity image (C) Color-coded fluorescence lifetime image of cells dyed with 12HNBO (1-hydroxy-2-naphthoic benzoxazole)

In Figure 11, 70% had a lifetime of about 500 ps while the remaining had a lifetime of 2.4 ns. The mean lifetime was approximately 1.1 nanoseconds. 12HNBO fluorescence signal is distinct from autofluorescence and is somewhat punctate,

congregating in to pockets of fluorescence. The signal appears to be mostly excluded from the nucleus.

3.3 2-hydroxy-3-naphthoic benzothiazole (23HNBT)

2-hydroxy-3-naphthoic benzothiazole was synthesized from 2-hydroxy-3-naphthoic acid and 2-aminothiophenol according to Scheme 5.

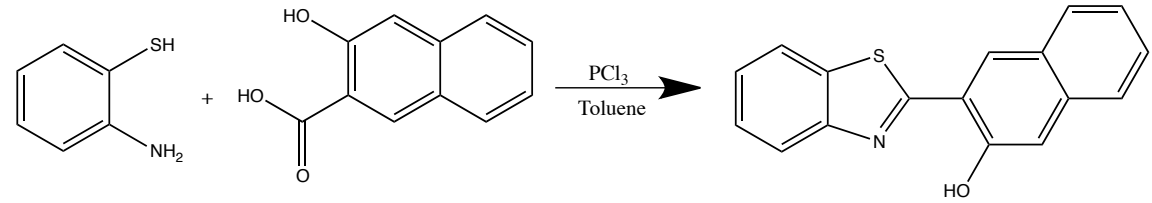

2-aminothiophenol 2-hydroxy-3-naphthoic acid 2-hydroxy-3-naphthoic benzothiazole

Scheme 5: Synthesis of 2-hydroxy-3-naphthoic benzothiazole

The absorbance, excitation, and emission spectra were taken in DMSO. Major absorbance peaks were observed at 260, 271, 282, and 331 nm. Excitation peaks occurred at 398 and 484 nm.

23HNBT	Absorbance	Excitation	Emission
Wavelengths (nm)	260, 271, 282, 331	398, 484	438, 573

Table 3: Absorbance, Excitation, and Emission peaks for 2-hydroxy-3-naphthoic benzothiazole (23HNBT)

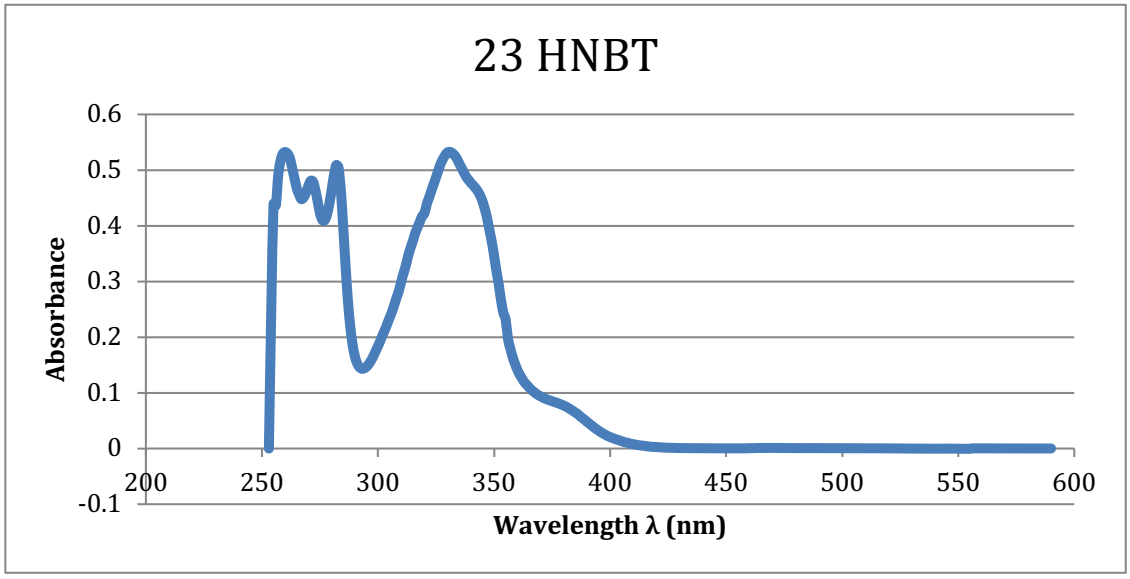

Figure 13: Absorbance spectrum of 2-hydroxy-3-napthnoic benzothiazole in DMSO

The absorbance and excitation spectra did not overlap completely and so, in effort to use a single wavelength with which to excite both 23HNBO and 23HNBT (avoiding unnecessary laser adjustments), the 2-photon wavelength initially chosen was 780 nm.

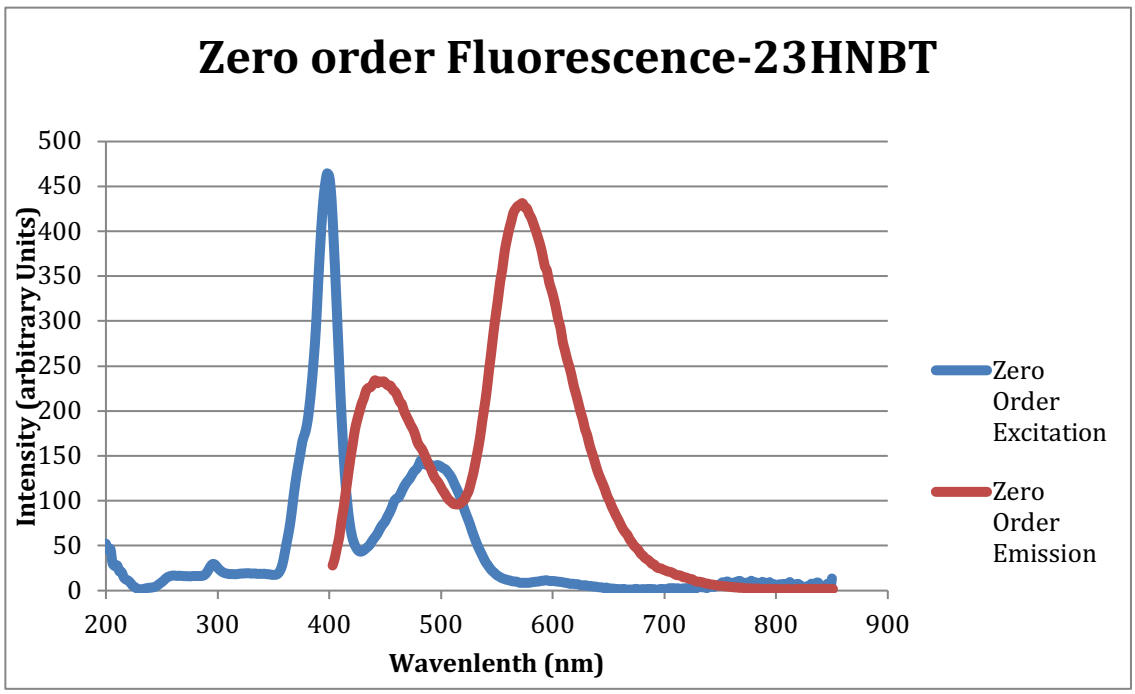

Figure 14: Zero order fluorescent excitation and emission spectra of 2-hydroxy-3-napthnoic benzothiazole (HNBT)

However, neither dye responded to this wavelength with a fluorescent signal distinct from that of autofluorescence. A second attempt was made using a wavelength of 760 nm with the same result. Finally, at a 735 nm wavelength, 23HNBT was observed as a distinct signal from autofluorescence. No significant signal was observed from 23HNBO at this wavelength or the previous two.

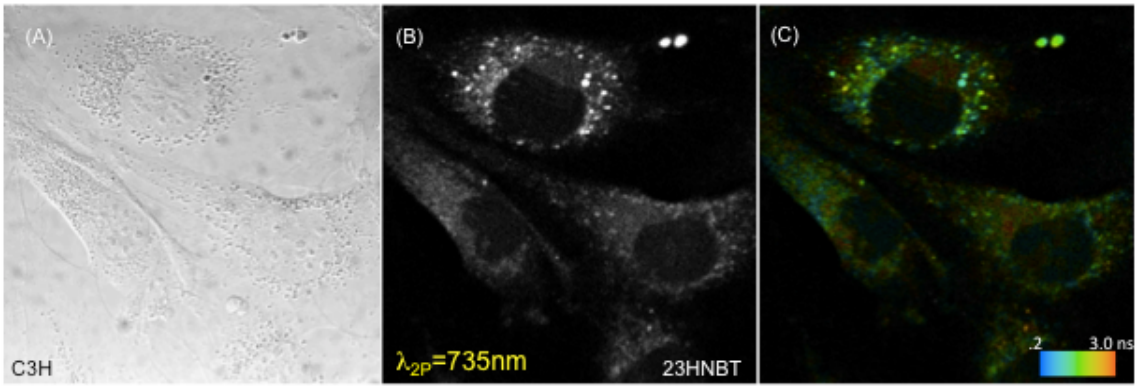

Figure 15: (A) DIC image (B) Intensity image (C) Color-coded fluorescence lifetime image of cells dyed with 23HNBT (2-hydroxy-3-naphthoic benzothiazole)

23HNBT displays biexponential fluorescence lifetime decay, indicating at least two environments within the cell. The dye is excluded from the nucleus. In Figure 15, 62% of the fluorescence signal decayed after 460 ps and 38% after 2.4 ns. The mean time was approximately 1.2 ns. In Figure 16, 71% of the signal decayed over 440 ps and the remaining 29% after 1.2 ns. The mean time was 1.2 ns per pixel.

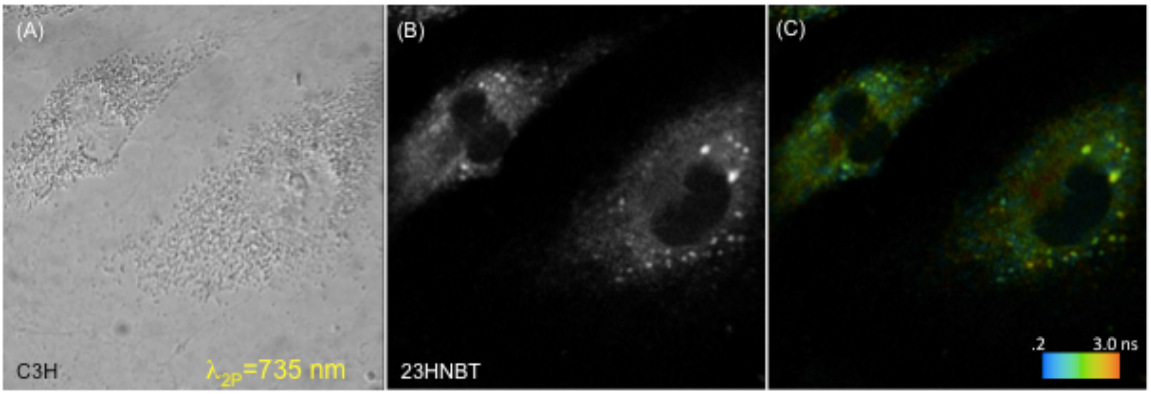

Figure 16: (A) DIC image (B) Intensity image (C) Color-coded fluorescence lifetime image of cells dyed with 23HNBT (2-hydroxy-3-naphthoic benzothiazole)

3.4 2-hydroxy-3-naphthoic benzoxazole (23HNBO)

This compound was synthesized from 2-hydroxy-3-naphthoic acid and 2-aminophenol according to Scheme 6.

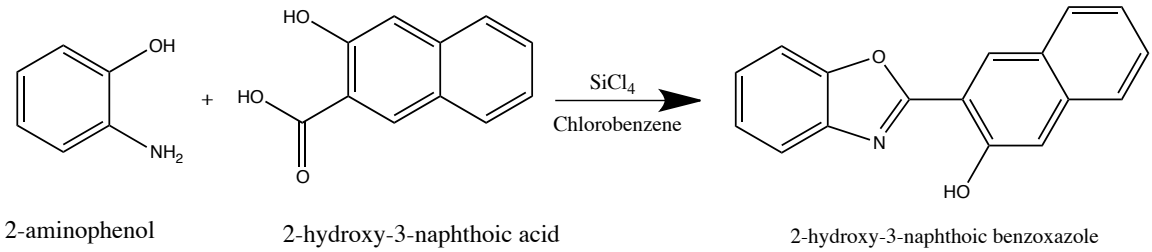

Scheme 6: Synthesis of 2-hydroxy-3-naphthoic benzoxazole (23HNBO)

The final compound of the four, 23HNBO, proved to be the most elusive. The ESIPT characteristics of this compound are more noticeable from its spectra given that the absorbance peaks in no way coincide with the excitation spectra.

23HNBO	Absorbance	Excitation	Emission
Wavelengths (nm)	260, 271, 282, 331	398, 481	567

Table 4: Absorbance, Excitation, and Emission peaks for 2-hydroxy-3-naphthoic benzoxazole (23HNBO)

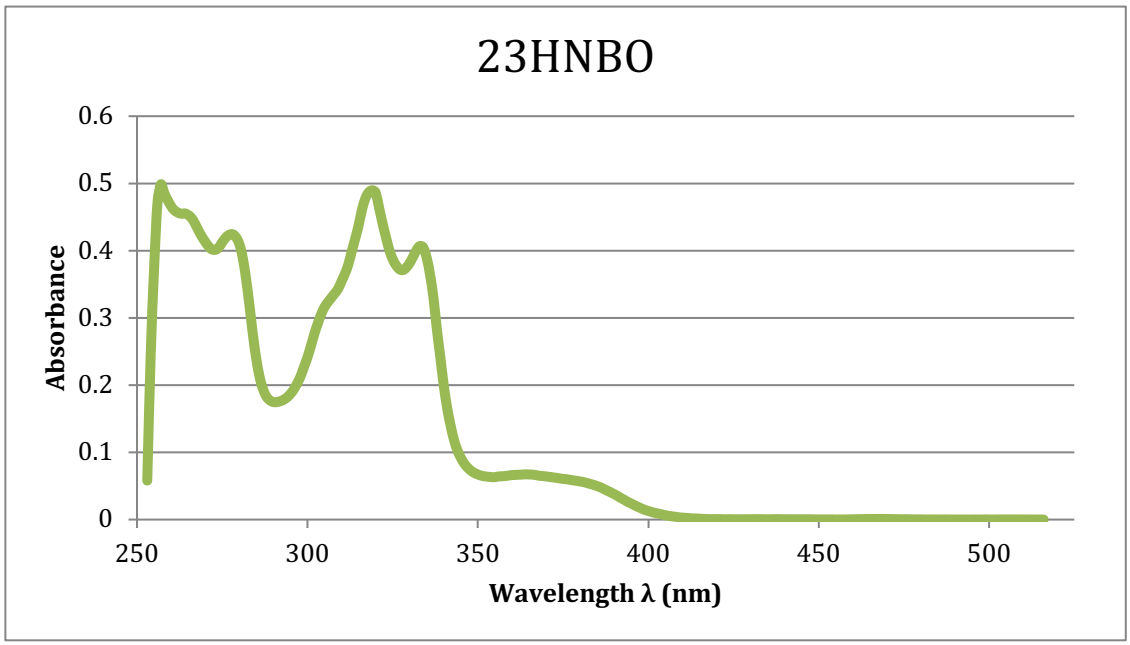

Figure 17: Absorbance spectrum of 2-hydroxy-3-naphthoic benzoxazole in DMSO

However, since the laser cannot be tuned to such low wavelengths as 700 nm, we were unable to test the dye under optimal conditions with respect to the absorbance spectrum. Therefore, we attempted to get as close as we could to a wavelength within the absorption spectrum, using 760 nm. However, there was no signal greater than that of autofluorescence. Then a wavelength of 950 nm was used in an attempt to use a wavelength within the excitation spectrum to excite the molecule. However, this too proved fruitless as no signal was observed that was distinct from the autofluorescence of the cells. Since the theoretical Log P was calculated to be the same for 12HNBO as

23HNBO, the molecule was probably present within the cell even if it was undetectable given either of the excitation wavelengths.

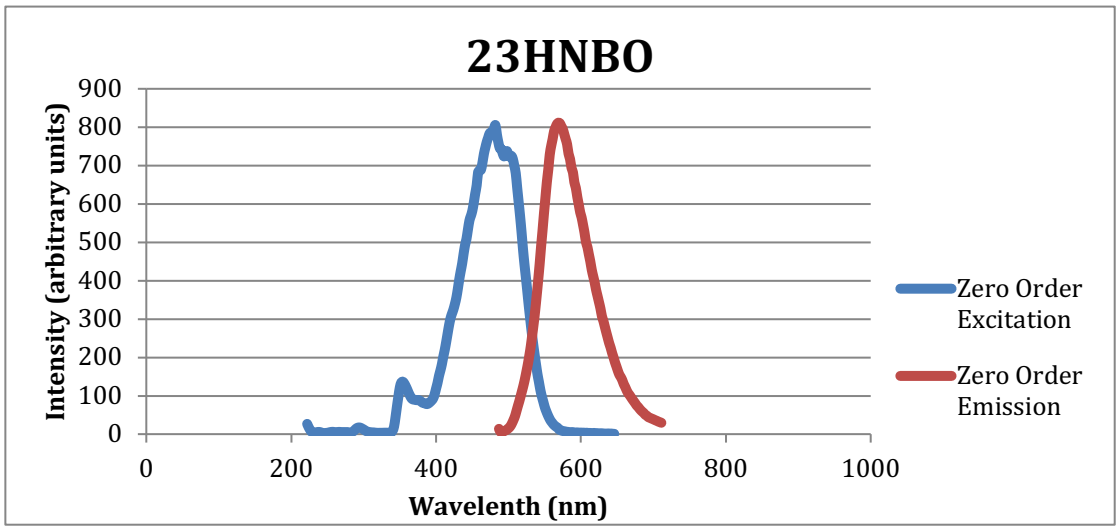

Figure 18: Zero Order Fluorescence Excitation and Emission Spectra of 2-hydroxy-3-naphthoic benzoxazole (HNBO) in DMSO

In Figure 19, the average lifetime per pixel was 1.7 ns. The decay was bi-exponential with 62% at 270 ps and 38% at 2.7 ns. The fluorescence signal was not distinguishable from that of cellular autofluorescence.

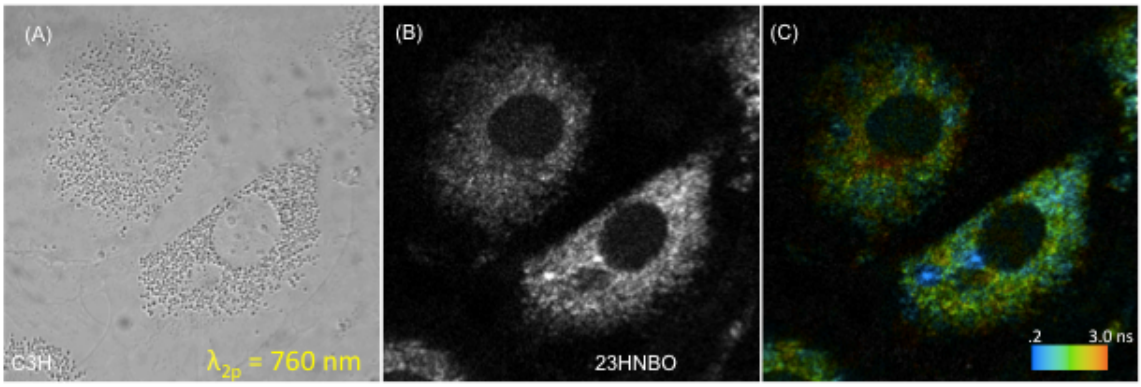

Figure 19: a) DIC image of mouse fibroblast cells with 2-hydroxy 3-naphthanoic benzoxazole b) FLIM image of same fibroblast cells c) FLIM image with color differentiation of fluorescence lifetime

3.5 Computational Chemistry Study

The compounds studied have the possibility for ESIPT which is connected to the ability to transfer a hydrogen in the excited state. An indication for this is the ability of a compound to develop intramolecular hydrogen bonding. At the same time, the spectroscopic study is done in a variety of solvents and it was important to know the solvent effect on the photochemistry of the compounds (Figure 20). The 2,1-substitution pattern on the naphthyl substituent was also included for completeness.

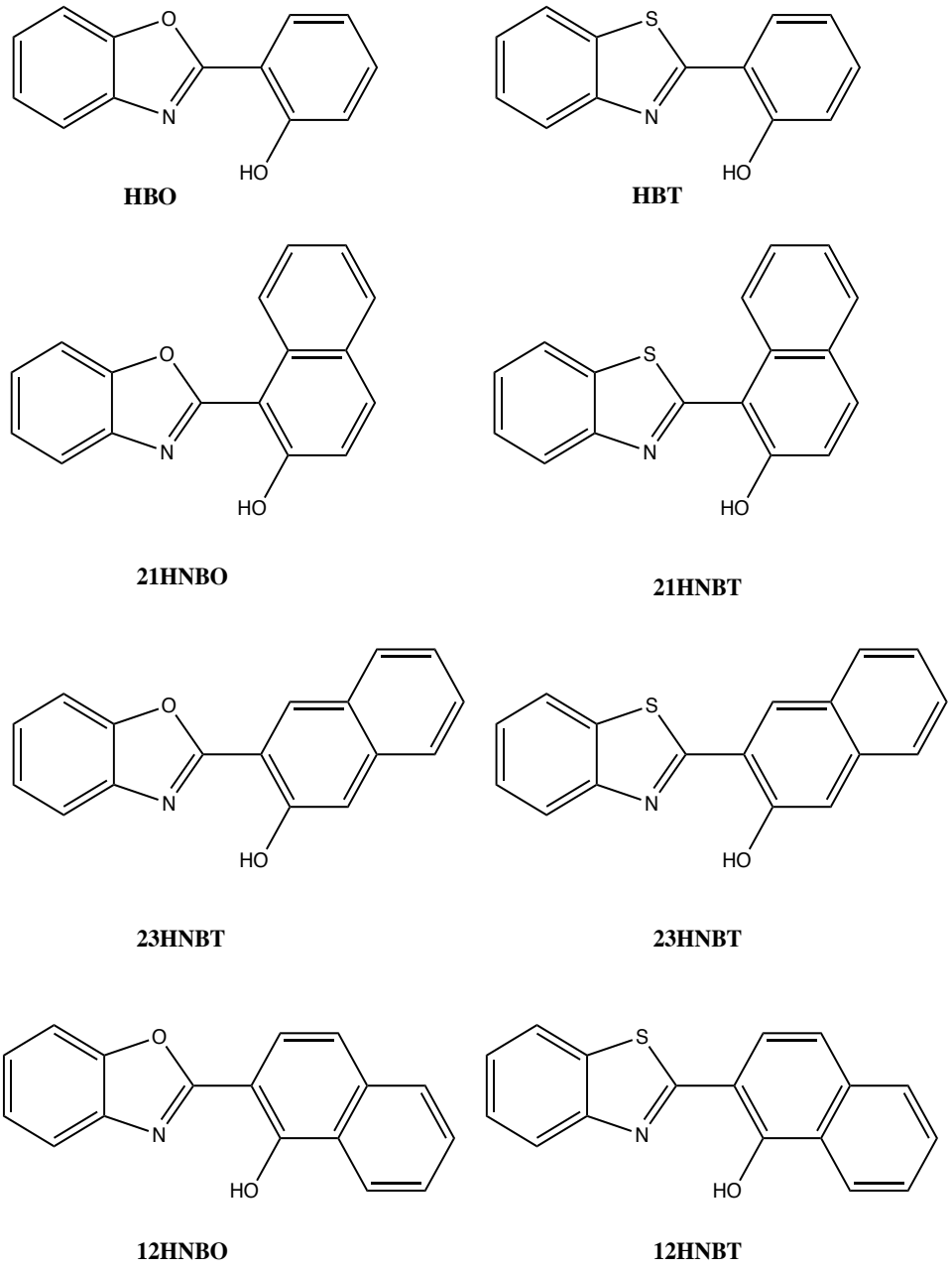

Figure 20: Compounds studied by computational methods.

Density Functional theory (DFT) has enabled researchers to get highly accurate computational data for compounds, time-dependent DFT (TDDFT) allows for the calculation of photochemical properties such as absorption and emission spectra, and

optimization of the excited state structure. [39–42] The computational models used here was the robust, well-known B3LYP functional and the 6-311++G** basis set, which is a good compromise for the size of the molecules. Solvent effects were accounted for by placing the molecules in cavity within the solvent reaction field (SCRF) using the Polarizable Continuum Model (PCM).

The molecules studied are fairly rigid, they allow for a variation in dihedral angles only at two places, the connection between the ring systems and the hydroxy group. This can give rise to four conformers in each case, assuming that the preferred alignment of the two ring systems is coplanar (Figure 21).

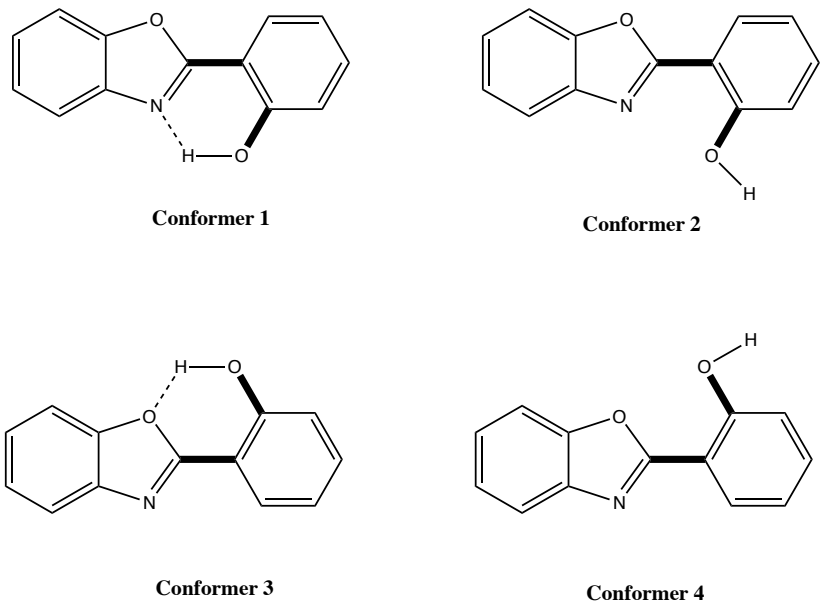

Figure 21: Conformers of HBO. Bonds with variable dihedral angles are marked in bold.

Conformers 1 and 2 can develop a hydrogen bond between the hydroxy group with nitrogen and oxygen respectively. In the case of the sulfur analog HBT the hydrogen bond in conformer 3 is not possible. A conformer analysis was performed using two methods, first to optimize the structures of the four conformers, second to rotate the rings and do an otherwise relaxed optimization for the rest of the molecule. The structures and relative energies of the conformers are shown in Figure 22 for dichloromethane as a solvent and in Figure 23 for water as a solvent.

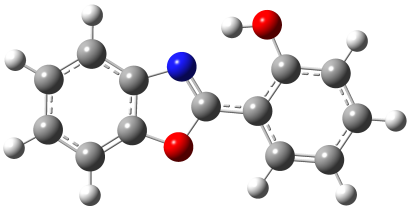	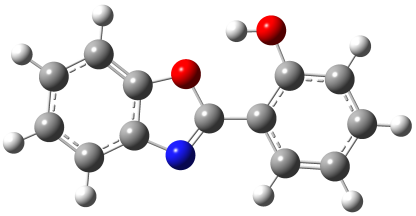
Conformer 1: 0.00 kcal/mol	Conformer 2: +4.79 kcal/mol
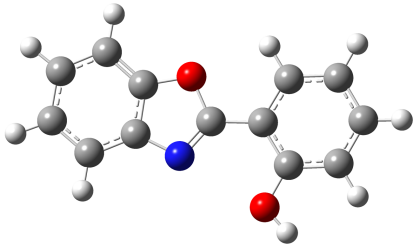	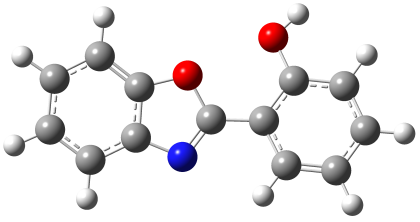
Conformer 3: +8.07 kcal/mol	Conformer 4: +8.03 kcal/mol

Figure 22: Conformers and relative energies of HBO in dichloromethane as a solvent. The relative energies are calculated using the Zero-Point Energy corrected electronic energies.

All conformers have a coplanar structure of the rings with only slight deviations in some cases. Conformer 1, with the hydrogen bond to the nitrogen is the lowest in energy. Conformer 2 with the other possible hydrogen bond is higher by 4.79 kcal/mol. The two non-hydrogen bonded conformers are higher in energy by roughly 8 kcal/mol. Conformer 1 would be overwhelmingly dominant in solution. All other conformers would be present at much less than 1%.

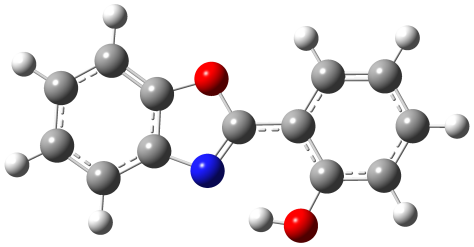	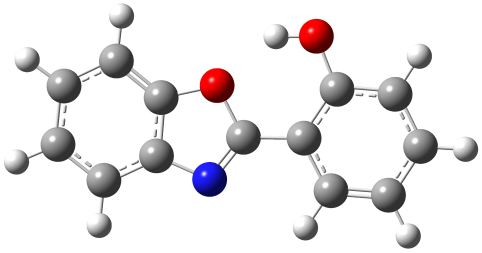
Conformer 1: 0.00 kcal/mol	Conformer 2: +4.64 kcal/mol

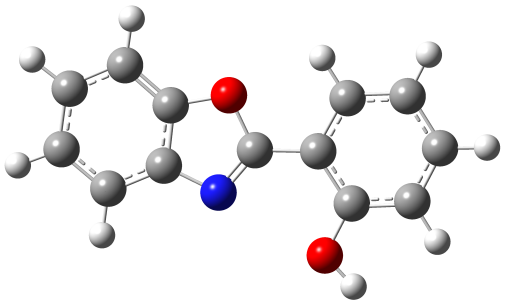	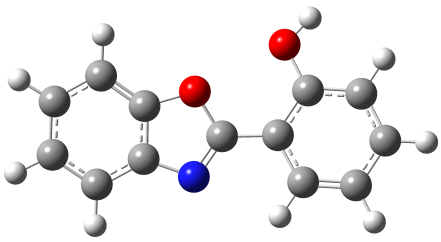
Conformer 3: +7.39 kcal/mol	Conformer 4: +7.50 kcal/mol

Figure 23: Conformers and relative energies of HBO in water as a solvent. The relative energies are calculated using the Zero-Point Energy corrected electronic energies.

The same picture as seen in the case of dichloromethane as a solvent, is observed for the calculations with water as a solvent. The relative energies of the non-hydrogen bonded conformers are slightly lower due to the higher polarity of the solvent. The SCRF-PCM model does not consider explicit hydrogen bonding unless the solvent is included in the molecule explicitly.

The same study was performed for the sulfur analog HBT (Figures 25 and 26) in dichloromethane and water as solvents respectively.

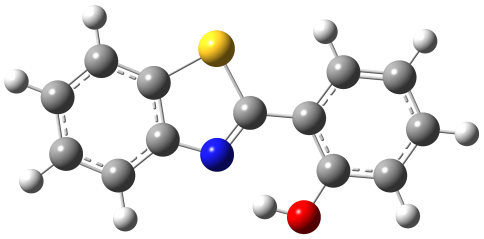	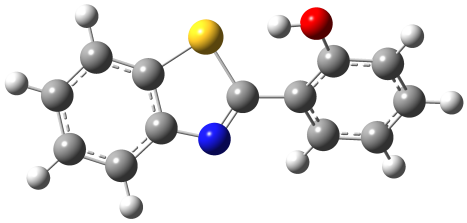
Conformer 1: 0.00 kcal/mol	Conformer 2: +8.37 kcal/mol
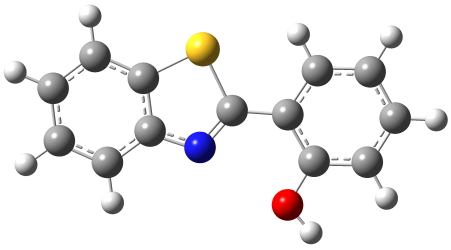	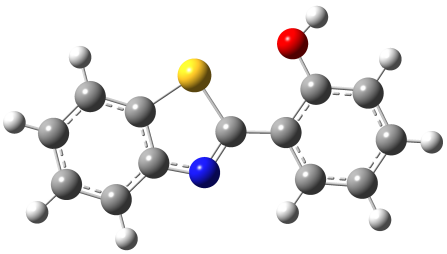
Conformer 3: +9.63 kcal/mol	Conformer 4: +6.35 kcal/mol

Figure 24: Conformers and relative energies of HBT in dichloromethane as a solvent. The relative energies are calculated using the Zero-Point Energy corrected electronic energies.

In the case of the sulfur-containing compound, conformer 2 cannot engage in hydrogen bonding, in fact the structure is approximately 36° from planarity. The hydrogen atom is avoiding the sulfur for steric reasons. Because of this the relative energy is much higher than the oxygen analog. The other structures are coplanar since there is not a major steric

interaction. Conformers 3 and 4 are higher because of the lack of hydrogen bonding, conformer 4 being significantly lower, conformer 2 is higher in energy than conformer 4 because of the nonplanarity.

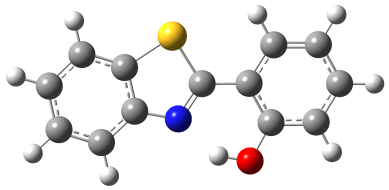	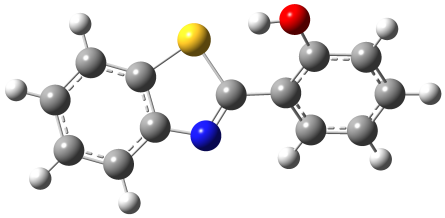
Conformer 1: 0.00 kcal/mol	Conformer 2: +8.22 kcal/mol
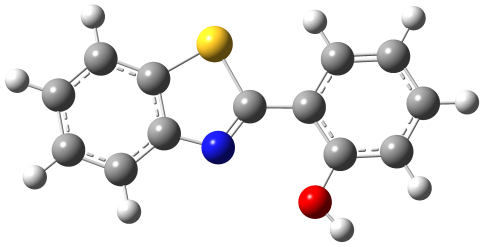	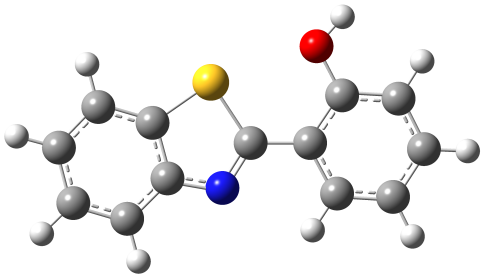
Conformer 3: +9.00 kcal/mol	Conformer 4: +6.01 kcal/mol

Figure 25: Conformers and relative energies of HBT in water as a solvent. The relative energies are calculated using the Zero-Point Energy corrected electronic energies.

The picture in water as a solvent in very similar to dichloromethane. Conformer 2 cannot engage in hydrogen bonding and is by 37° out of plane to avoid steric interaction

between sulfur and hydrogen. The discrepancy of hydrogen bonded versus not hydrogen bonded structures (here conformer 1 vs conformers 2,3, and 4) is lowered because of the higher polarity of the solvent.

For the naphthyl derivatives, no explicit conformer analysis was performed since the basic pattern is assumed to be the same, especially for the 1,2 and 2,3 substitutions, for the 2,1 isomer, there is an additional steric interaction because of how the naphthyl group is aligned (Figure 26).

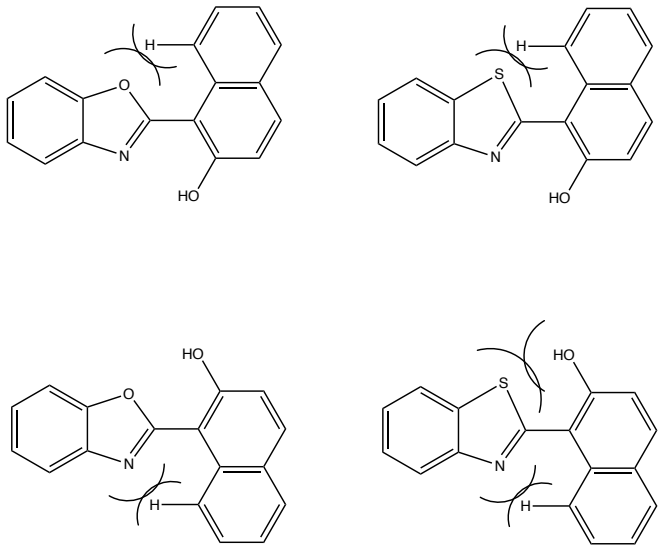

Figure 26: Steric Interactions in the 2,1 substituted naphthyl derivatives.

Instead, to evaluate the effect of rotation around the bond that connects the two ring systems together, a relaxed scan was performed by changing the dihedral angle by 10° and letting the rest of the molecule adjust to the dihedral angle. The results are shown in Figure 27.

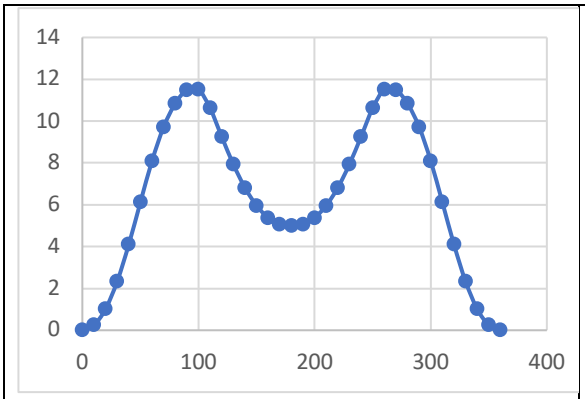	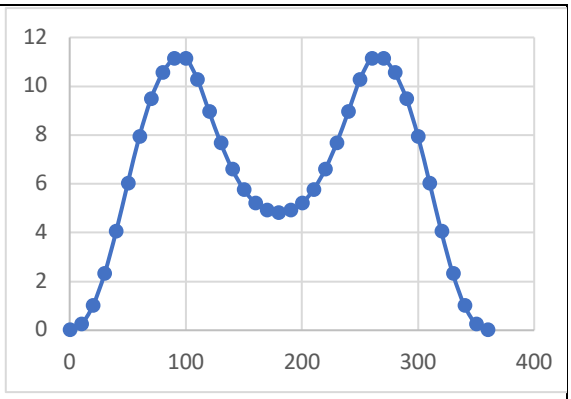
HBO-DCM	HBO-water
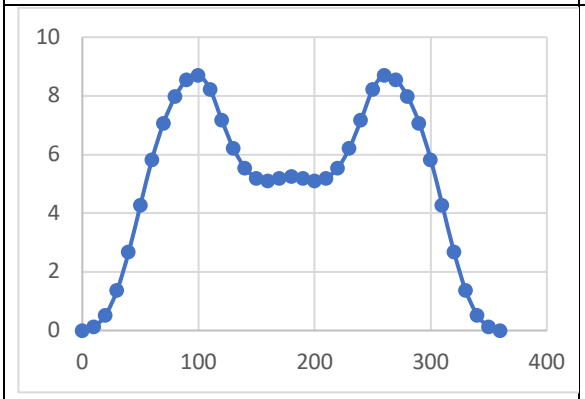	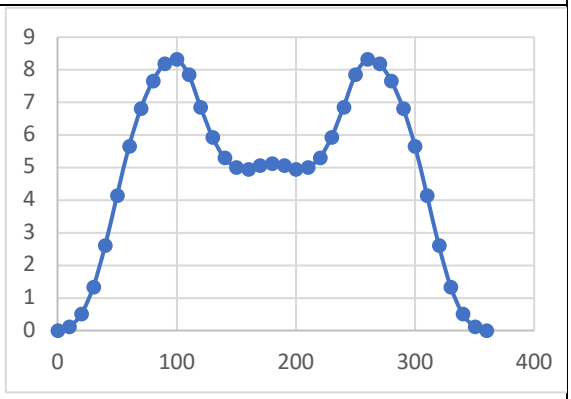
21HNBO-DCM	21HNBO-water
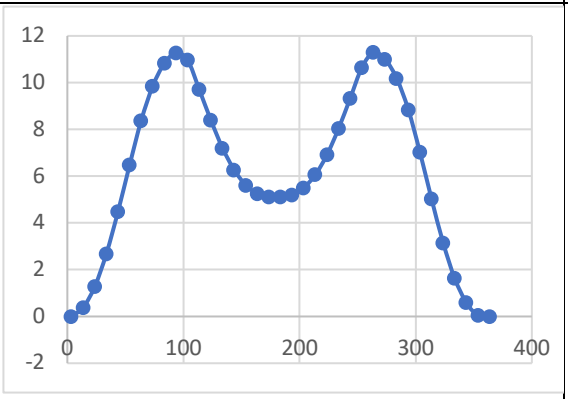	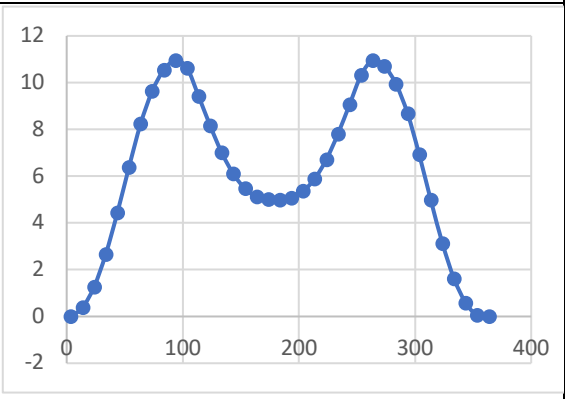
23HNBO-DCM	23HNBO-water

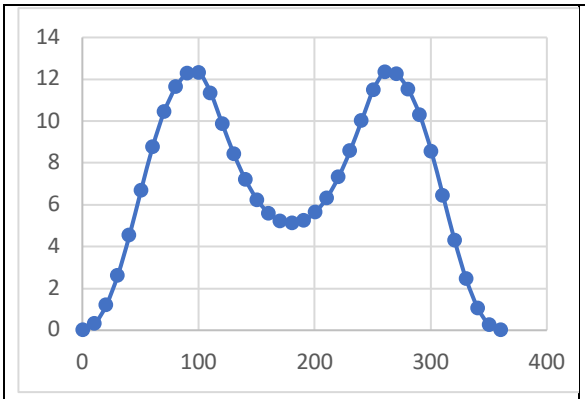

12HNBO-DCM

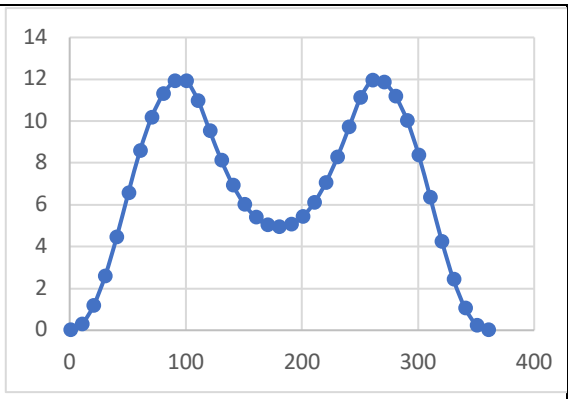

12HNBO-water

Figure 27: Relaxed scans of the oxygen analogues in dichloromethane (DCM) and water as solvent. The x-axis is the dihedral angle and the y-axis is the relative energy to the lowest conformation.

The scans show maxima in energy at the 90 and 270° angles where the two pi systems are perpendicular to each other and have no interaction. The lowest minimum is when the hydroxyl group is engaged in hydrogen bonding with the nitrogen and a higher local minimum is observed when the hydroxyl group engages in hydrogen bonding with oxygen. The differences in the minima correspond very well with the differences calculated for the specific conformers. The 21HNBO compound has a steric interaction between a naphthyl hydrogen and the OH group and therefore shows no minimum at 180°, but two minima that are close to planarity but avoid steric interaction at angles below and above 180°. In general, the energies of conformations outside of planarity are not as high in energy for water, since the increased polarity accommodates the fact that polar groups are not engaged in hydrogen bonding. The same calculations were performed for the sulfur derivatives and are shown in Figure 28.

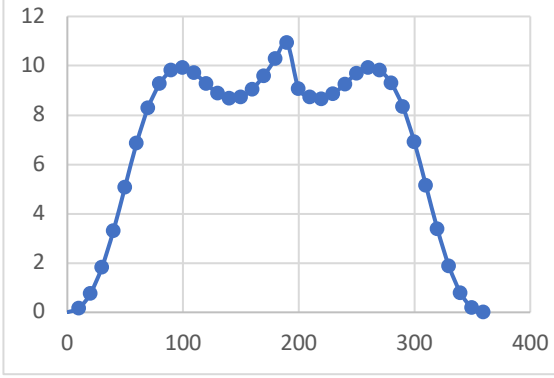	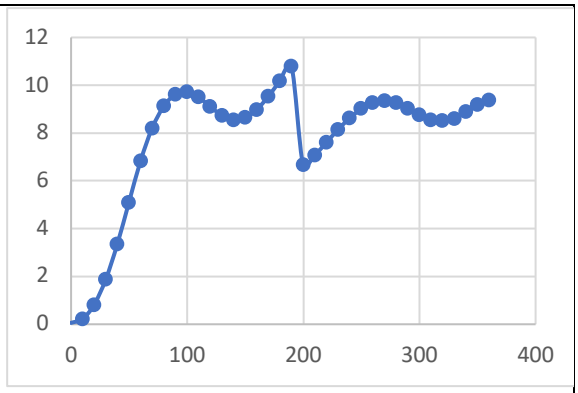
HBT-DCM	HBT-water
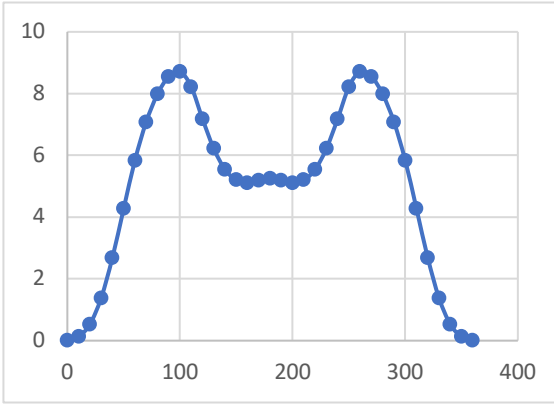	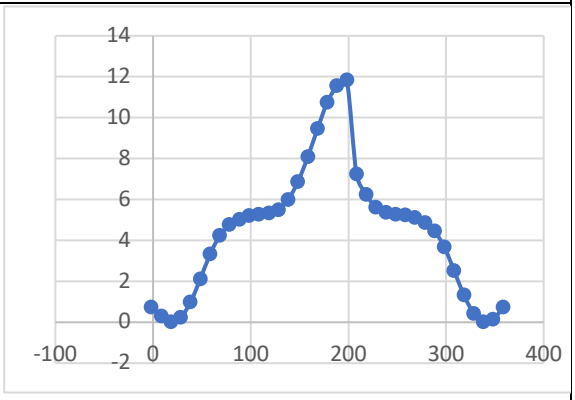
21HNBT-DCM	21HNBT-water
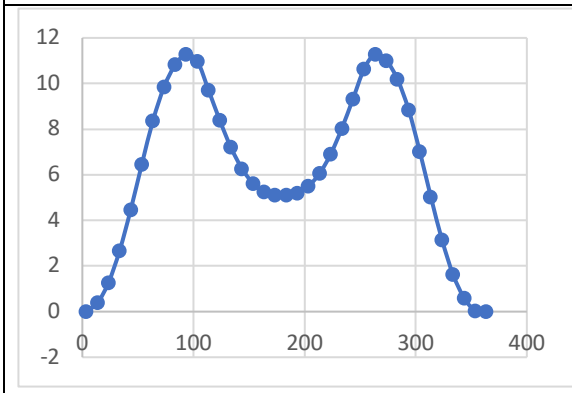	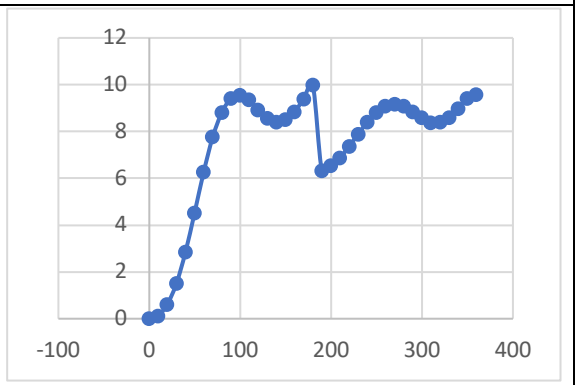
23HNBT-DCM	23HNBT-water

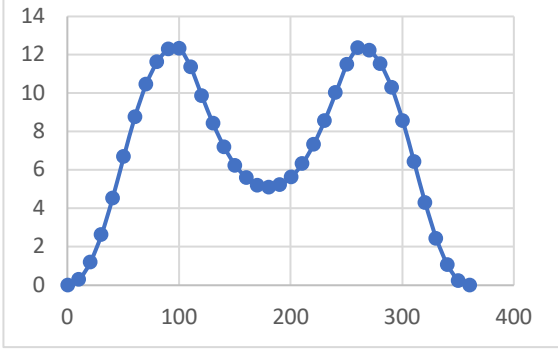

12HNBT-DCM

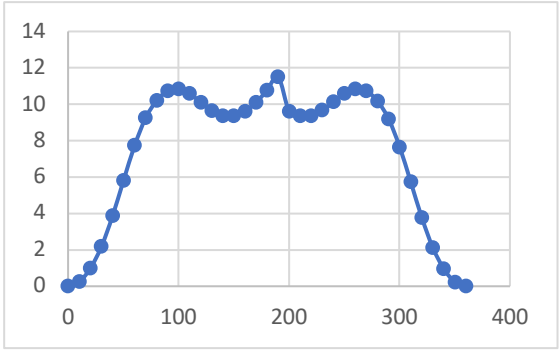

12HNBT-water

Figure 28: Relaxed scans of the sulfur analogues in dichloromethane (DCM) and water as solvent.

The scans of the sulfur compounds are characterized by the fact that there is no hydrogen bonding around 180* possible so that the OH group and sulfur are in an unfavorable steric interaction. The minimization process then turns the dihedral angle of the OH group and the second half of the curve is different than the first since the conformations are different. In the case of 21HNBT there is the additional steric strain with the orientation of the naphthyl group which results in an even higher maximum in energy. The curves can be symmetrized to show a shape that is closer to that of the oxygen compounds where the OH group does not turn and that are symmetrical because of two types of hydrogen bonding (Figure 29). The symmetrized figures are shown in Figure 30.

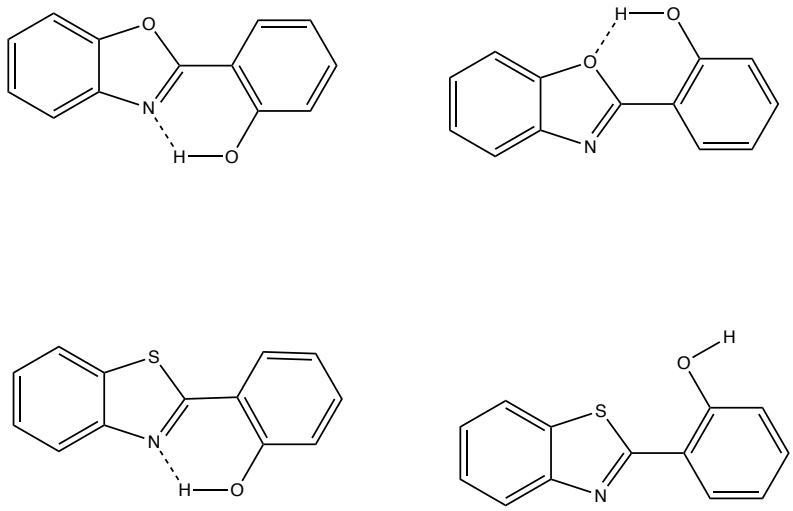

Figure 29. Two types of possible hydrogen bonding in the oxygen derivatives versus only one type in the sulfur derivatives

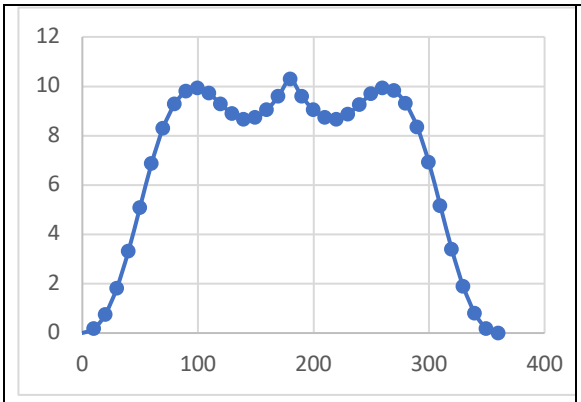

HBT-DCM

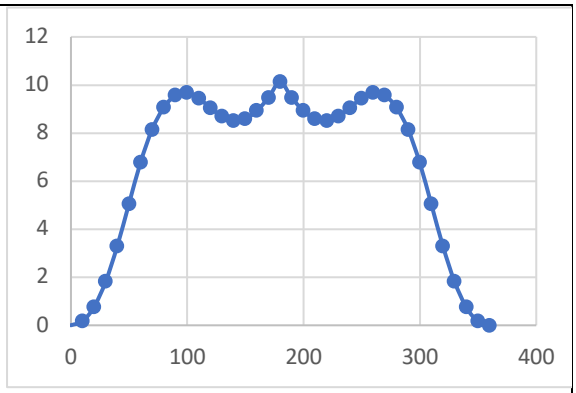

HBT-water

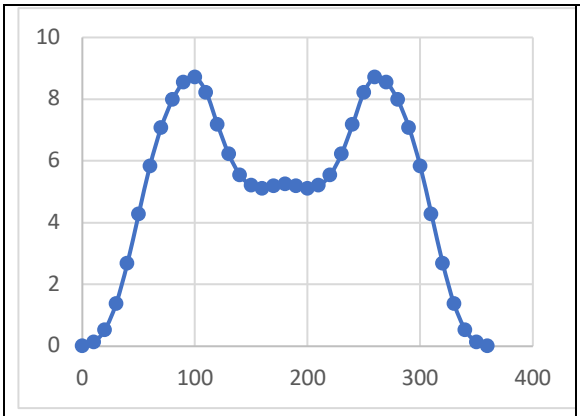

21HNBT-DCM

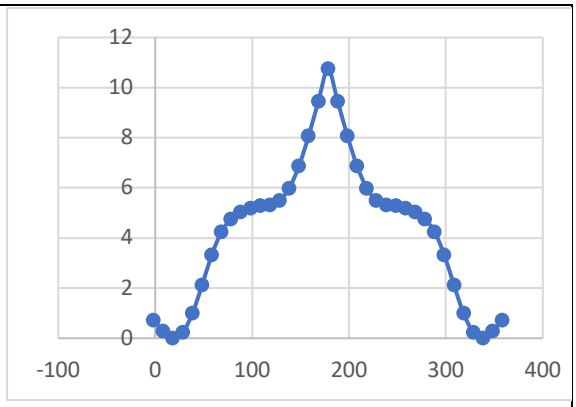

21HNBT-water

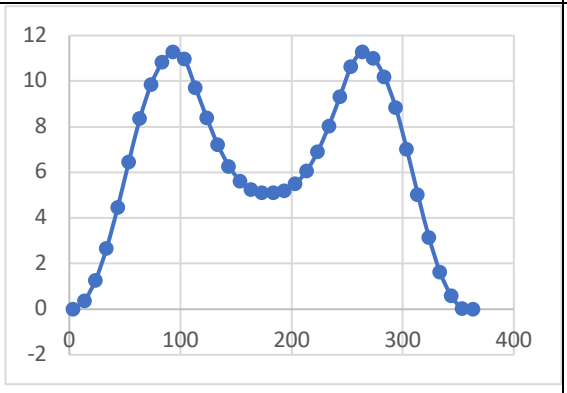

23HNBT-DCM

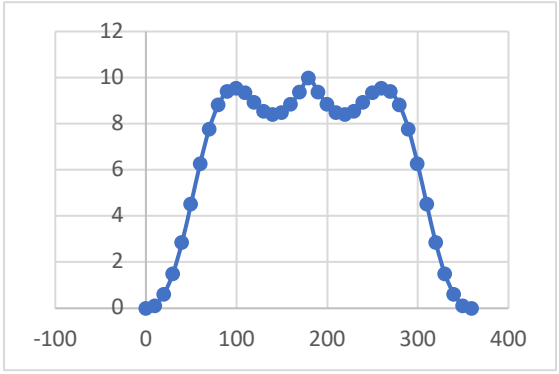

23HNBT-water

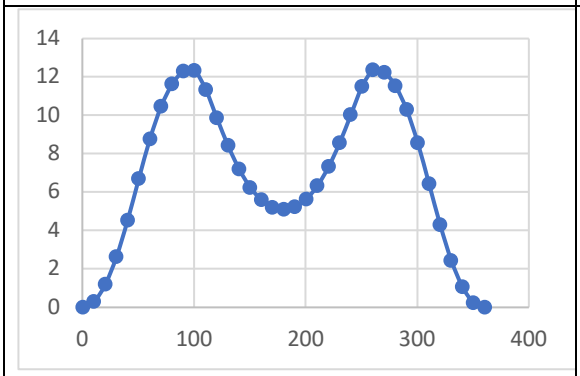

12HNBT-DCM

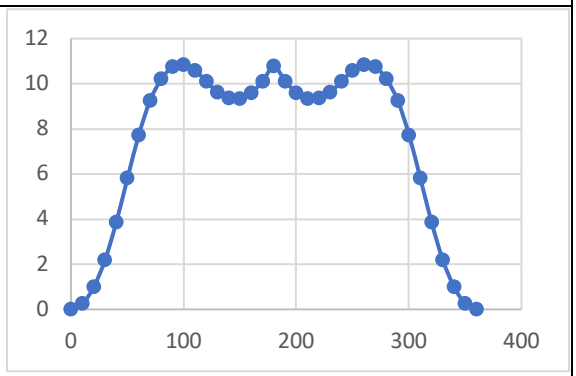

12HNBT-water

Figure 30: Relaxed scans of the sulfur analogues in dichloromethane (DCM) and water as solvent. The curves have been corrected in that they were symmetrized.

From these calculations and the energy difference between the lowest energy conformer it can be argued, that all molecules exist in a preferred conformer which connects the hydroxy group with the aromatic nitrogen function through a hydrogen bond, both in polar and nonpolar, protic and aprotic solvents. Therefore, the photochemical calculations will be performed with that single conformer for each compound. The compounds were optimized in geometry and it was verified that a local minimum was achieved using a frequency calculation that contained no negative frequencies. The computed UV-VIS spectra are shown in figures 31 and 32.

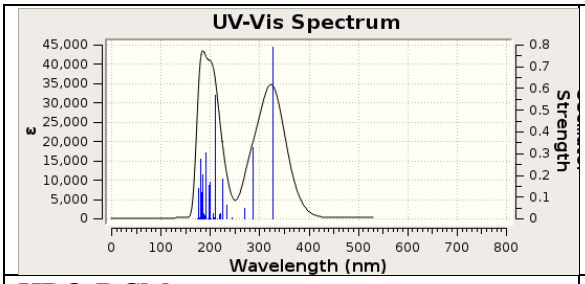

HBO-DCM

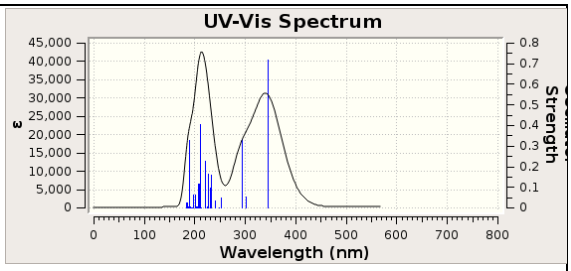

HBT-DCM

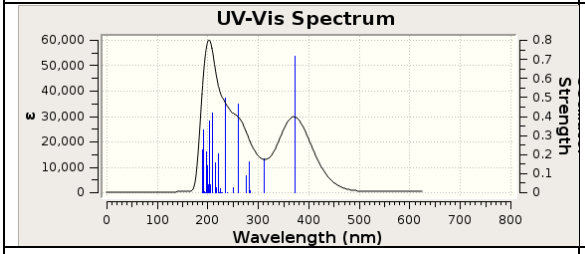

21HNBO-DCM

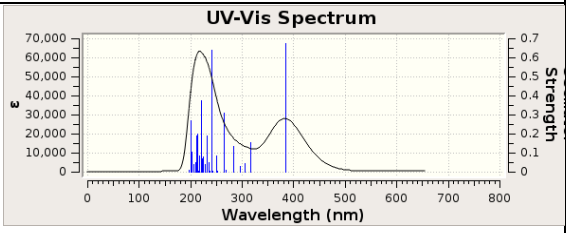

21HNBT-DCM

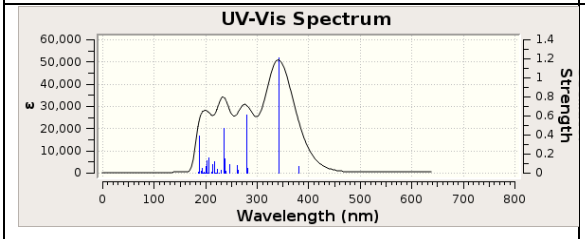

23HNBO-DCM

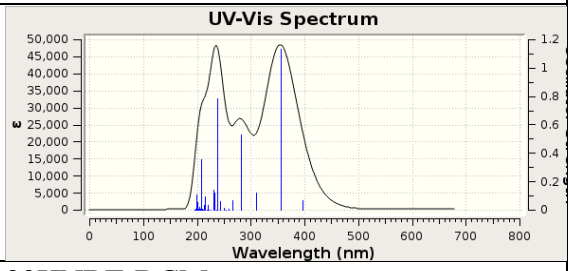

23HNBT-DCM

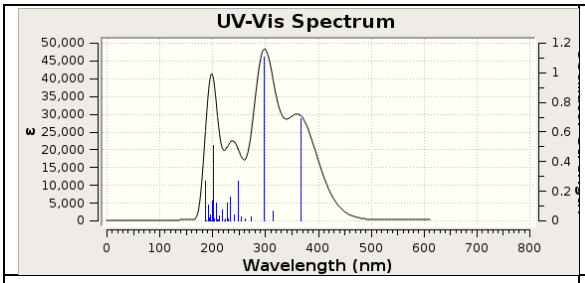	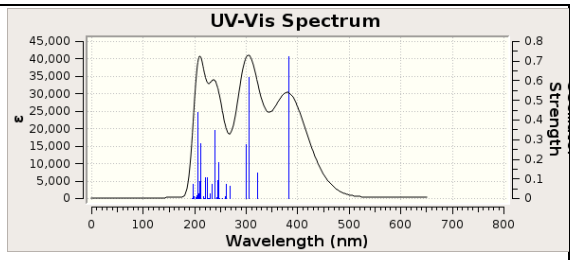
12HNBO-DCM	12HNBT-DCM

Figure 31. Calculated UV-VIS spectra in dichloromethane as solvent. The vertical lines are the absorptions calculated in the TD-DFT simulation.

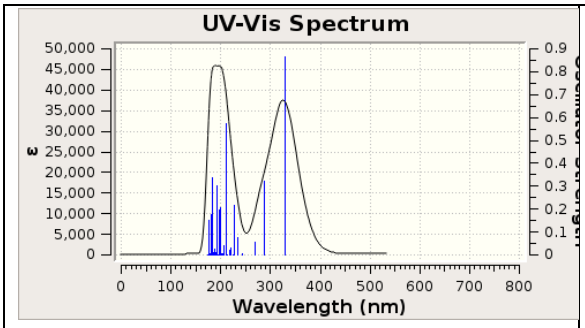	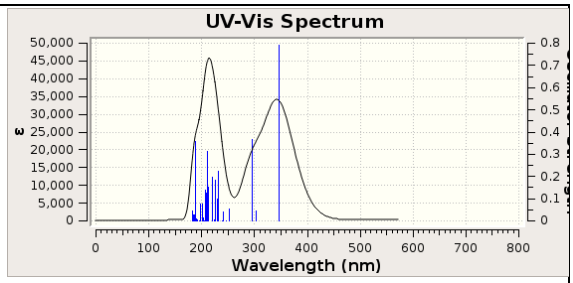
HBO-H2O	HBT- H2O
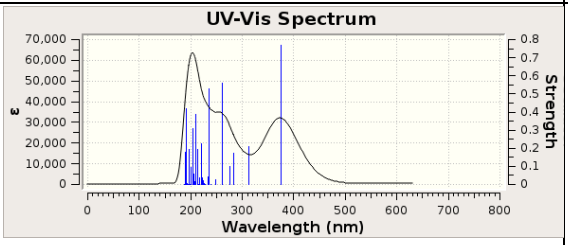	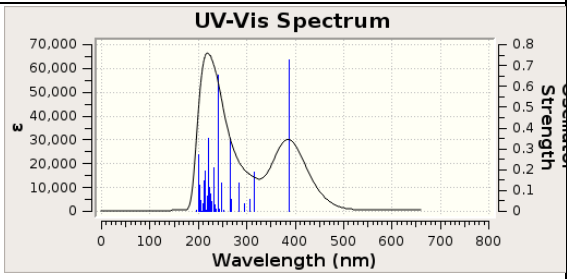
21HNBO- H2O	21HNBT- H2O

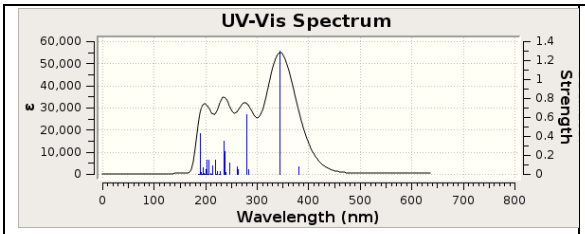

23HNBO- H2O

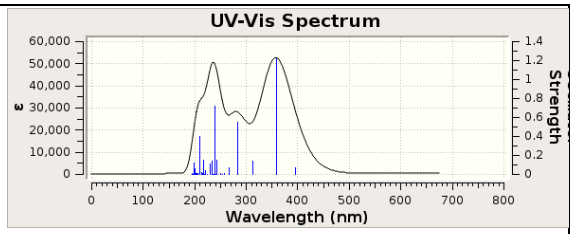

23HNBT- H2O

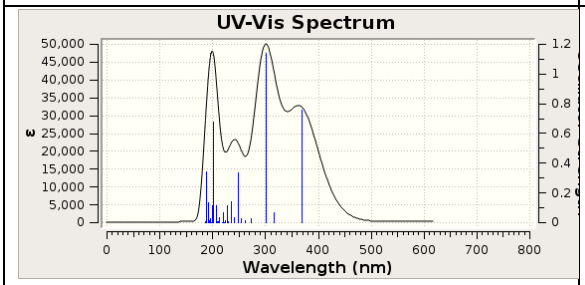

12HNBO- H2O

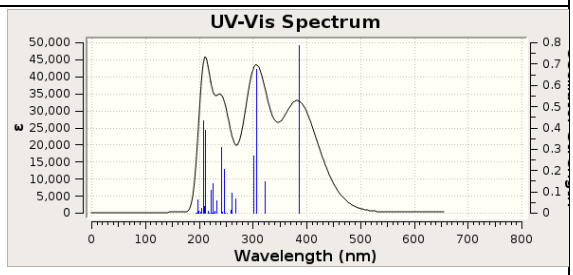

12HNBT- H2O

Figure 32: Calculated UV-VIS spectra in dichloromethane as solvent. The vertical lines are the absorptions calculated in the TD-DFT simulation.

As a general observation, there is not much of a solvatochromic effect seen in these results, the dichloromethane and water solvent results are almost identical for each compound. For reasons of simplicity it makes sense to continue with only the dichloromethane data in the further discussion.

When comparing each oxygen-containing compound to its sulfur analogue it can be seen that the spectrum is analogous with a bathochromic shift (Figure 33). If sulfur is included in the aromatic ring, it participates more strongly in the aromatic system with its lone pair, especially in the LUMO,[43–45] similar to the case of thiophene vs. furane. The energy gap between the orbitals where the electron is originating and where it is placed in the excited state is smaller which shifts the absorption to a longer wavelength (Table 5).

In the case of the 23HNBO and 23HNBT, the longest wavelength is weak as indicated by the oscillator strength of that peak.

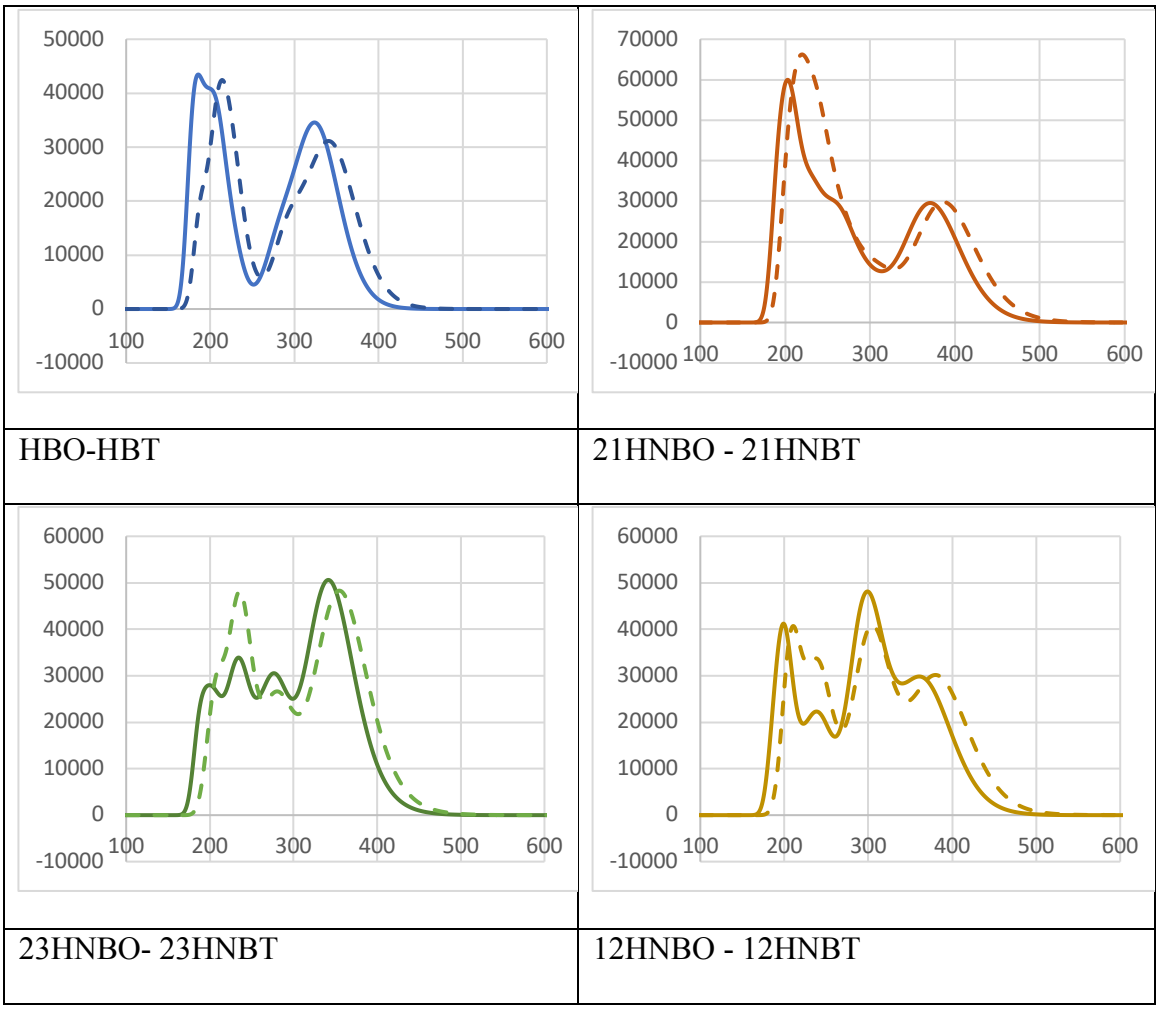

Figure 33: Comparison of the absorption spectra of oxygen (solid lines) and sulfur compounds (dashed lines) in dichloromethane.

Compound	Calculated wavelength [nm]	Observed wavelength [nm]
HBO	327.82	356 [46]
HBT	344.74 372.32	364 [46]
21HNBT	387.14	
12HNBO	380.38	415
12HNBT	396.12	443
23HNBO	366.52	331
23HNBT	383.19	484, 398

Table 5: Calculated first absorption wavelengths of the eight compounds

Unlike in the case of the complexed boron derivatives that were studied previously [47–50], the agreement of calculation and experiment is not as good. This may be due to the fact that the OH group can interact with solvent molecules and other fluorophore molecules which is not accounted for in the computations. Another possibility is the choice of the density functional. Whereas B3LYP has proven very robust in producing correct geometries, it is not as robust as other functionals. Since in our own previous studies it was very reliable, we chose to use it in this study since both, reliable geometries and fairly good prediction of absorptions were needed.

Overall, the computational results give a good insight of what conformers are important in solution, namely only one, which is stabilized by hydrogen bonding. The steric demand of the 2,1 substituted naphthyl derivate makes it difficult for it to be planar and so it presents a special case in this series of compounds. When the oxygen is

substituted with sulfur, not only does the hydrogen bonding not occur, but now there is steric repulsion between the OH group and the sulfur.

The prediction of the absorption spectra is not as accurate as for systems where boron is introduced instead of hydrogen between the phenolic oxygen and nitrogen, albeit important trends in the longest wavelength absorption with consideration of size of the π system and heteroatom sulfur or oxygen are accurate.

Conclusion

Four fluorescent compounds (12HNBO, 12HNBT, 23HNBO and 23HNBT) were presented and were studied for use in cellular imaging. This study was building on the synthesis of light-emitting boron-containing fluorophores previously in our group. Simpler homologues of these compounds have been reported to complex with metal ions and fluorescently label β-amyloid plaques in Alzheimer's disease research.

The photochemical hallmark of these and related fluorophores is their Excited-State Intramolecular Proton Transfer (ESIPT) tautomerization. With this in mind, we investigated each of the compounds using 2-Photon Fluorescence Lifetime Imaging Microscopy (2P-FLIM) and Differential Interference Contrast (DIC) microscopy. Three of the compounds were found to have a fluorescence signal distinct from that of the autofluorescence inherent in the cells; the remaining compound (23HNBO) was not found to have any distinctive fluorescence signal above that of autofluorescence under the wavelengths available for experimentation with 2P-FLIM. Two of the compounds, 12HNBO and 23HNBT were excluded from the nucleus. Some 12HNBT fluorescence

signal was observed within the nucleus and also exhibited an extended lifetime in two regions surrounding the nucleus of a, possibly, mitotic cell.

These dyes do not display as high intensity as some other, previously known, dyes such as fluorescein or members of the BODIPY family, having fluorescence efficiency lower than commercial dyes. The quantum inefficiency of these compounds is likely due to the tautomerization undergone by these compounds in an excited state. There appears to be no specific location to which the dyes are attracted and transport into the cell is likely passive. However, most notably, one of the compounds appears to be incorporated in the cell nucleus during mitosis. In all cases the fluorescence lifetimes were bi-exponential, which indicates the presence of at least two distinct chemical environments for the fluorophore. Future studies will refine the conditions of cell incubation and photochemical studies further and examine the cell location in more detail. The computational results complement the experimental findings and give supporting information about the molecules in solution.

Bibliography

(1) Lakowicz, J. R. *Principles of Fluorescence Spectroscopy*, 3rd ed.; Springer US, 2006.
(2) Manders, E. M. M.; Verbeek, F. J.; Aten, J. A. Measurement of Co-localization of Objects in Dual-colour Confocal Images. *J. Microsc.* **1993**, *169* (3), 375–382. https://doi.org/10.1111/j.1365-2818.1993.tb03313.x.
(3) Carlson, J. Strategic Synthetic Color Tuning of a Family of Simple Azole Based Luminescent Organoboron Compounds. MS Thesis, University of Minnesota, 2010.
(4) Toonstra, C. Tunable Luminescent Boron Complexes. MS Thesis, University of Minnesota, 2011.
(5) Kiprof, P.; C. Carlson, J.; R. Anderson, D.; N. Nemykin, V. Systematic Color Tuning of a Family of Luminescent Azole -Based Organoboron Compounds Suitable for OLED Applications. *Dalton Trans.* **2013**, *42* (42), 15120–15132. https://doi.org/10.1039/C3DT51853A.
(6) Herschel John Frederick William. IV. ’Αμόρφωγa, No. I.— on a Case of Superficial Colour Presented by a Homogeneous Liquid Internally Colourless. *Philos. Trans. R. Soc. Lond.* **1845**, *135*, 143–145. https://doi.org/10.1098/rstl.1845.0004.
(7) Herschel John Frederick William. V. ’Αμόρφωγa, No. II.— on the Epipölic Dispersion of Light, Being a Supplement to a Paper Entitled, “On a Case of Superficial Colour Presented by a Homogeneous Liquid Internally Colourless.". *Philos. Trans. R. Soc. Lond.* **1845**, *135*, 147–153. https://doi.org/10.1098/rstl.1845.0005.
(8) Stokes George Gabriel. XXX. On the Change of Refrangibility of Light. *Philos. Trans. R. Soc. Lond.* **1852**, *142*, 463–562. https://doi.org/10.1098/rstl.1852.0022.
(9) Hurtubise, R. J. *Phosphorimetry: Theory, Instrumentation, and Applications*; VCH Publishers: New York, N.Y, 1990.
(10) Wang, S. Luminescence and Electroluminescence of Al(III), B(III), Be(II) and Zn(II) Complexes with Nitrogen Donors. *Coord. Chem. Rev.* **2001**, *215* (1), 79–98. https://doi.org/10.1016/S0010-8545(00)00403-3.
(11) Wu, Q.; Esteghamatian, M.; Hu, N.-X.; Popovic, Z.; Enright, G.; Tao, Y.; D’Iorio, M.; Wang, S. Synthesis, Structure, and Electroluminescence of BR2q (R = Et, Ph, 2-Naphthyl and q = 8-Hydroxyquinolato). *Chem. Mater.* **2000**, *12* (1), 79–83. https://doi.org/10.1021/cm990372a.
(12) Zhao, S.-B.; Wang, S. Luminescence and Reactivity of 7-Azaindole Derivatives and Complexes. *Chem. Soc. Rev.* **2010**, *39* (8), 3142–3156. https://doi.org/10.1039/c001897j.
(13) Deperasińska, I.; Gryko, D. T.; Karpiuk, E.; Kozankiewicz, B.; Makarewicz, A.; Piechowska, J. Low-Temperature Spectra of the Analogues of 10-Hydroxybenzo[h]Quinoline as an Indication of Barrierless ESIPT. *J. Phys. Chem. A* **2012**, *116* (49), 12049–12055. https://doi.org/10.1021/jp309340x.
(14) Kwon, J. E.; Park, S. Y. Advanced Organic Optoelectronic Materials: Harnessing Excited-State Intramolecular Proton Transfer (ESIPT) Process. *Adv. Mater.* **2011**, *23* (32), 3615–3642. https://doi.org/10.1002/adma.201102046.

(15) Mutai, T.; Sawatani, H.; Shida, T.; Shono, H.; Araki, K. Tuning of Excited-State Intramolecular Proton Transfer (ESIPT) Fluorescence of Imidazo[1,2-a]Pyridine in Rigid Matrices by Substitution Effect. *J. Org. Chem.* **2013**, *78* (6), 2482–2489. https://doi.org/10.1021/jo302711t.
(16) Sinha, S.; Chowdhury, B.; Ghosh, P. A Highly Sensitive ESIPT-Based Ratiometric Fluorescence Sensor for Selective Detection of Al^{3+}. *Inorg. Chem.* **2016**, *55* (18), 9212–9220. https://doi.org/10.1021/acs.inorgchem.6b01170.
(17) Zhang, X.; Ma, W.-W. Amplified Excited State Intramolecular Proton Transfer Fluorescence of Butterfly-Shaped Bis-2,6-Dibenzothiazolylphenol. *Methods Appl. Fluoresc.* **2017**, *5* (2), 024013. https://doi.org/10.1088/2050-6120/aa73b2.
(18) Wu, K.-C.; Lin, Y.-S.; Yeh, Y.-S.; Chen, C.-Y.; Ahmed, M. O.; Chou, P.-T.; Hon, Y.-S. Design and Synthesis of Intramolecular Hydrogen Bonding Systems. Their Application in Metal Cation Sensing Based on Excited-State Proton Transfer Reaction. *Tetrahedron* **2004**, *60* (51), 11861–11868. https://doi.org/10.1016/j.tet.2004.09.102.
(19) Vdovin, A.; Sepioł, J.; Jasny, J.; Kauffman, J. M. Excited State Proton Transfer in Jet-Cooled 2,5-Di-Ž2-Benzoxazolyl/ Phenol. **1998**, 9.
(20) Forés, M.; Duran, M.; Solà, M.; Adamowicz, L. Excited-State Intramolecular Proton Transfer and Rotamerism of 2-(2‘-Hydroxyvinyl)Benzimidazole and 2-(2‘-Hydroxyphenyl)Imidazole. *J. Phys. Chem. A* **1999**, *103* (22), 4413–4420. https://doi.org/10.1021/jp9844765.
(21) Taylor, C. A.; El-Bayoumi, M. A.; Kasha, M. Excited-State Two-Proton Tautomerism In Hydrogen-Bonded N-Heterocyclic Base. *Proc. Natl. Acad. Sci.* **1969**, *63* (2), 253–260. https://doi.org/10.1073/pnas.63.2.253.
(22) Toele, P.; Zhang, H.; Glasbeek, M. Femtosecond Fluorescence Anisotropy Studies of Excited-State Intramolecular Double-Proton Transfer in [2,2‘-Bipyridyl]-3,3‘-Diol in Solution. *J. Phys. Chem. A* **2002**, *106* (15), 3651–3658. https://doi.org/10.1021/jp0134446.
(23) Kletskii, M. E.; Millov, A. A.; Metelitsa, A. V.; Knyazhansky, M. I. Role of Structural Flexibility in the Fluorescence and Photochromism of Salicylideneaniline: The General Scheme of the Phototransformations. *J. Photochem. Photobiol. Chem.* **1997**, *110* (3), 267–270. https://doi.org/10.1016/S1010-6030(97)00196-2.
(24) Anthony, K.; Brown, R. G.; Hepworth, J. D.; Hodgson, K. W.; May, B.; West, M. A. Solid-State Fluorescent Photophysics of Some 2-Substituted Benzothiazoles. *J. Chem. Soc. Perkin Trans. 2* **1984**, *0* (12), 2111–2117. https://doi.org/10.1039/P29840002111.
(25) Pluta, M.; Maksymilian, P. *Advanced Light Microscopy*; Elsevier Amsterdam, 1988; Vol. 1.
(26) Pluta, M. Nomarski’s DIC Microscopy: A Review. In *Phase Contrast and Differential Interference Contrast Imaging Techniques and Applications*; International Society for Optics and Photonics, 1994; Vol. 1846, pp 10–26.
(27) Pluta, M. *Phase Contrast Microscopy*; SOC PHOTO-OPT INSTRUM ENG PO BOX 10, BELLINGHAM, WA 98227-0010, 1993.

(28) Kleinschmidt, J.; Graness, A. Determination of the Quantum Yields of Photochemical Reactions by Means of Absorption Saturation Measurements I: Quantum Yields of Photochemical Intramolecular Proton Transfer Reactions in 2-(2′,4′-Dinitrobenzyl)-Pyridine Solutions. *J. Photochem.* **1983**, *22* (1), 25–31. https://doi.org/10.1016/0047-2670(93)80004-9.
(29) Tanaka, K.; Kumagai, T.; Aoki, H.; Deguchi, M.; Iwata, S. Application of 2-(3,5,6-Trifluoro-2-Hydroxy-4-Methoxyphenyl)Benzoxazole and -Benzothiazole to Fluorescent Probes Sensing PH and Metal Cations. *J. Org. Chem.* **2001**, *66* (22), 7328–7333. https://doi.org/10.1021/jo010462a.
(30) Rodríguez-Rodríguez, C.; Sánchez de Groot, N.; Rimola, A.; Álvarez-Larena, Á.; Lloveras, V.; Vidal-Gancedo, J.; Ventura, S.; Vendrell, J.; Sodupe, M.; González-Duarte, P. Design, Selection, and Characterization of Thioflavin-Based Intercalation Compounds with Metal Chelating Properties for Application in Alzheimer's Disease. *J. Am. Chem. Soc.* **2009**, *131* (4), 1436–1451. https://doi.org/10.1021/ja806062g.
(31) Kafafi, Z. H. *Organic Electroluminescence*; CRC Press, 2005.
(32) Halford, E. OLED TV Gets Ready For Prime Time. *Chem. Eng. News Arch.* **2004**, *82* (21), 13. https://doi.org/10.1021/cen-v082n021.p013a.
(33) Kalinowski, J. *Organic Light-Emitting Diodes: Principles, Characteristics & Processes*; Marcel Dekker, 2005.
(34) *Organic Light-Emitting Materials and Devices*.
(35) Kumar, A.; Kumar, D. Synthesis and Antimicrobial Activity of Metal Complexes from 2-(1'/2'-Hydroxynaphthyl)Benzoxazoles. *Arkivoc* **2007**, *2007* (14), 117. https://doi.org/10.3998/ark.5550190.0008.e12.
(36) *SPCImage 3.8 Data Analysis Software for Fluorescence Lifetime Imaging Microscopy. Becker and Hickle GmbH 2012*.
(37) Frisch, M. J.; Trucks, G. W.; Schlegel, H. B.; Scuseria, G. E.; Robb, M. A.; Cheeseman, J. R.; Scalmani, G.; Barone, V.; Mennucci, B.; Petersson, G. A.; et al. *Gaussian~09 Revision A.1*.
(38) Frisch, M. J.; Trucks, G. W.; Schlegel, H. B.; Scuseria, G. E.; Robb, M. A.; Cheeseman, J. R.; Scalmani, G.; Barone, V.; Petersson, G. A.; Nakatsuji, H.; et al. *Gaussian 16 Revision B.01*; 2016.
(39) Zhao, X.; Chen, M. A TDDFT Study on the Singlet and Triplet Excited-State Hydrogen Bonding and Proton Transfer of 10-Hydroxybenzo[h]Quinoline (HBQ) and 7,9-Diiodo-10-Hydroxybenzo[h]Quinoline (DIHBQ). *Chem. Phys. Lett.* **2011**, *512* (1–3), 35–39. https://doi.org/10.1016/j.cplett.2011.07.003.
(40) Yang, P.; Zhao, J.; Wu, W.; Yu, X.; Liu, Y. Accessing the Long-Lived Triplet Excited States in Bodipy-Conjugated 2-(2-Hydroxyphenyl) Benzothiazole/Benzoxazoles and Applications as Organic Triplet Photosensitizers for Photooxidations. *J. Org. Chem.* **2012**, *77* (14), 6166–6178. https://doi.org/10.1021/jo300943t.
(41) Kantchev, E. A. B.; Norsten, T. B.; Sullivan, M. B. Time-Dependent Density Functional Theory (TDDFT) Modelling of Pechmann Dyes: From Accurate

Absorption Maximum Prediction to Virtual Dye Screening. *Org. Biomol. Chem.* **2012**, *10* (33), 6682. https://doi.org/10.1039/c2ob25806d.
(42) Jamorski Jödicke, C.; Lüthi, H. P. Time-Dependent Density Functional Theory (TDDFT) Study of the Excited Charge-Transfer State Formation of a Series of Aromatic Donor-Acceptor Systems. *J. Am. Chem. Soc.* **2003**, *125* (1), 252–264.
(43) Friedman, P.; Ferris, K. F. A Theoretical Study of the Aromaticity of Hypervalent Sulfur Heterocycles. *J. Mol. Struct. THEOCHEM* **1997**, *418* (2–3), 119–126. https://doi.org/10.1016/S0166-1280(96)05017-8.
(44) Palmer, M. H.; Findlay, R. H. The Electronic Structure of Some Sulphur-Containing Heterocycles. *Tetrahedron Lett.* **1972**, *13* (41), 4165–4168.
(45) Palmer, M. H.; Findlay, R. H. The Aromaticity of Heterocycles from Magnetic Susceptibility Anisotropy. *Tetrahedron Lett.* **1974**, *15* (3), 253–256.
(46) Tong, Y.-P.; Zheng, S.-L.; Chen, X.-M. Syntheses, Structures, Photoluminescence, and Theoretical Studies of a Class of Beryllium(II) Compounds of Aromatic N,O-Chelate Ligands. *Inorg. Chem.* **2005**, *44* (12), 4270–4275. https://doi.org/10.1021/ic0501059.
(47) Jacquemin, D.; Perpète, E. A.; Ciofini, I.; Adamo, C. Accurate Simulation of Optical Properties in Dyes. *Acc. Chem. Res.* **2009**, *42* (2), 326–334. https://doi.org/10.1021/ar800163d.
(48) Chibani, S.; Charaf-Eddin, A.; Le Guennic, B.; Jacquemin, D. Boranil and Related NBO Dyes: Insights From Theory. *J. Chem. Theory Comput.* **2013**, *9* (7), 3127–3135. https://doi.org/10.1021/ct400392r.
(49) Jacquemin, D.; Planchat, A.; Adamo, C.; Mennucci, B. TD-DFT Assessment of Functionals for Optical 0–0 Transitions in Solvated Dyes. *J. Chem. Theory Comput.* **2012**, *8* (7), 2359–2372. https://doi.org/10.1021/ct300326f.
(50) Jacquemin, D.; Perpete, E. A.; Scuseria, G. E.; Ciofini, I.; Adamo, C. TD-DFT Performance for the Visible Absorption Spectra of Organic Dyes: Conventional versus Long-Range Hybrids. *J. Chem. Theory Comput.* **2008**, *4* (1), 123–135. https://doi.org/10.1021/ct700187z.
(51) Quazi, Nurul H.; Hughes, Andrew B.; Tilley, Leann M. Synthesis of Novel Fluorescent Compounds. *Advances in Fluorescence Sensing Technology.* **1997**, *2980* (2), 270- 276.

Appendix: Additional Images

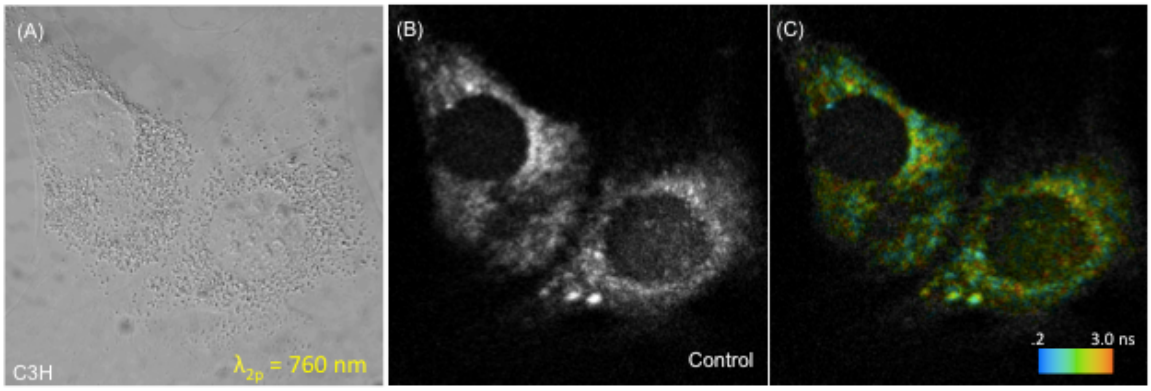

Figure 34: Control DIC and FLIM images for mouse fibroblast cells using 2-photon excitation at 760nm a) DIC microscopy b) FLIM image without color differentiation of lifetimes c) FLIM image with color coded fluorescence lifetimes

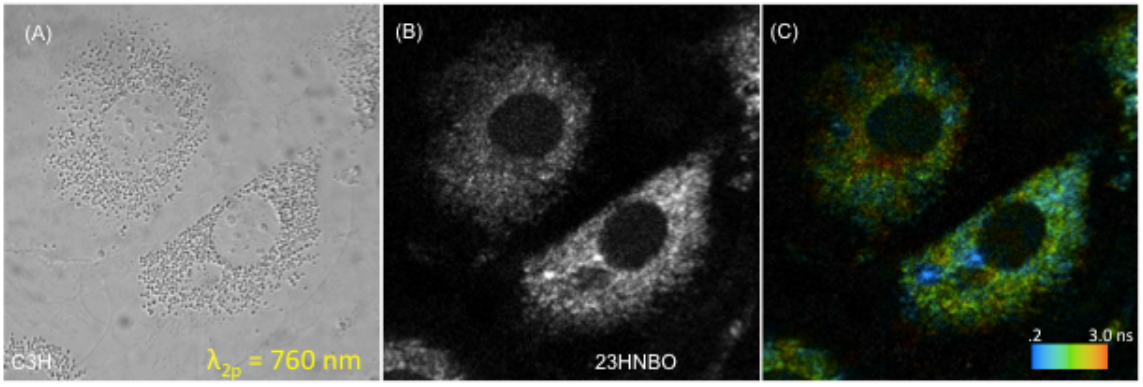

Figure 35: 2-hydroxy-3-naphthoic benzoxazole DIC and FLIM images a) DIC microscopy of mouse fibroblast b) FLIM image 2-photon excitation at 760 nm c) FLIM color coded lifetime image

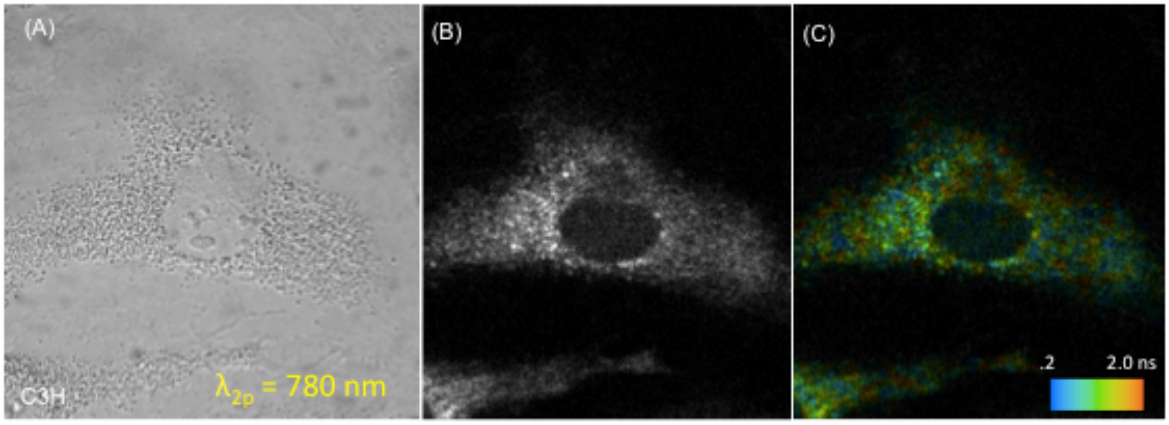

Figure 36: Control DIC and FLIM images for mouse fibroblast cells using 2-photon excitation at 780 nm a) DIC microscopy b) FLIM image without color differentiation of lifetimes c) FLIM image with color coded fluorescence lifetimes

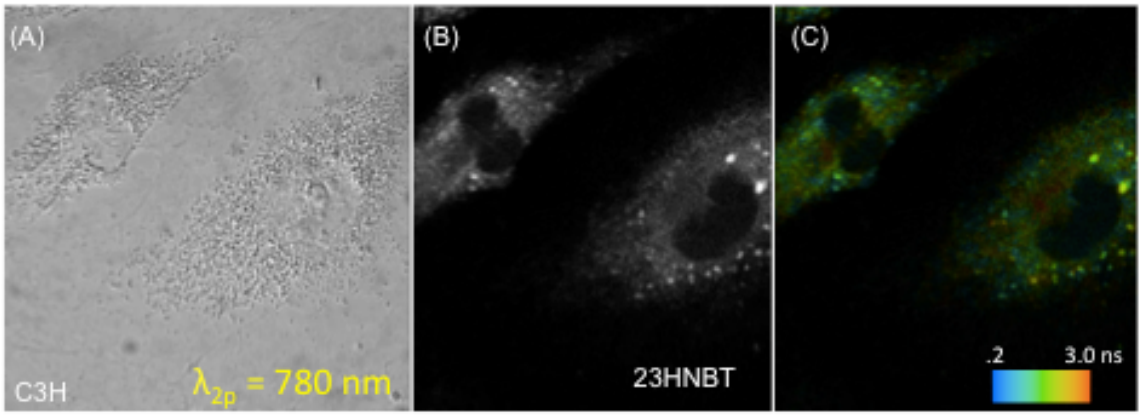

Figure 37: 2-hydroxy-3-naphthoic benzothiazole DIC and FLIM images a) DIC microscopy of mouse fibroblast b) FLIM image 2-photon excitation at 780 nm c) FLIM color coded lifetime image

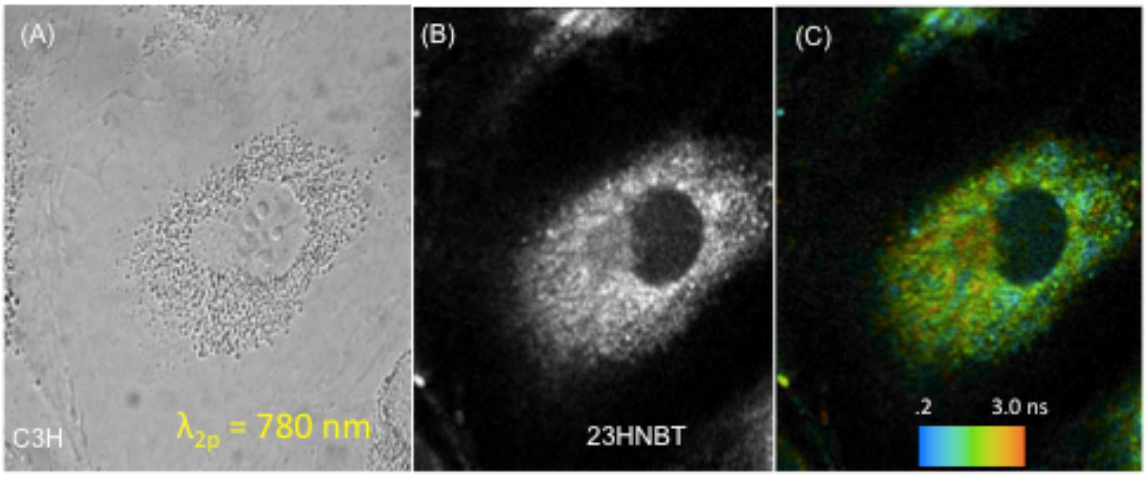

Figure 38: 2-hydroxy-3-naphthoic benzothiazole DIC and FLIM images a) DIC microscopy of mouse fibroblast b) FLIM image 2-photon excitation at 780 nm c) FLIM color coded lifetime image

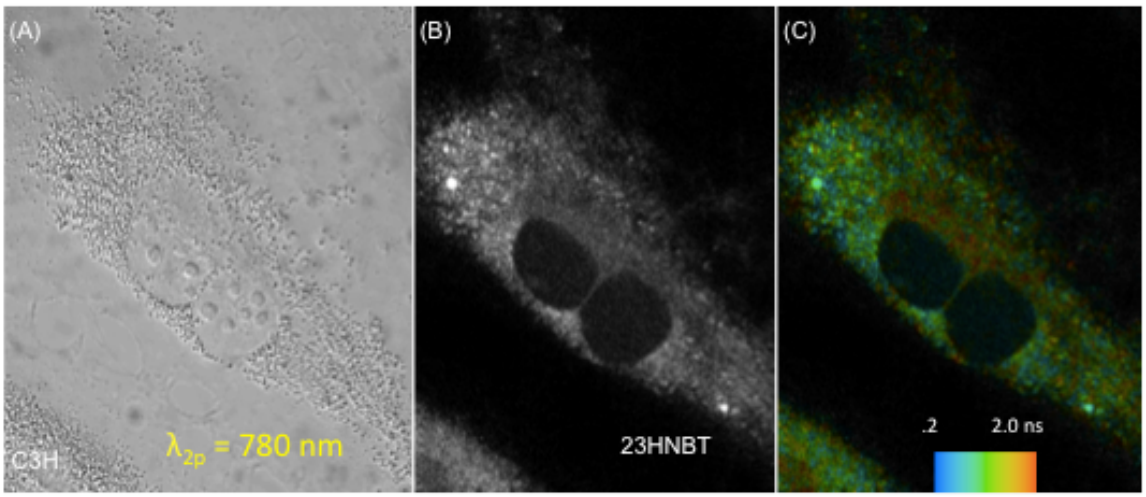

Figure 39: 2-hydroxy-3-naphthoic benzothiazole DIC and FLIM images a) DIC microscopy of mouse fibroblast b) FLIM image 2-photon excitation at 780 nm c) FLIM color coded lifetime image. This image seems to show the cell undergoing mitosis as it has two apparent nuclei. \

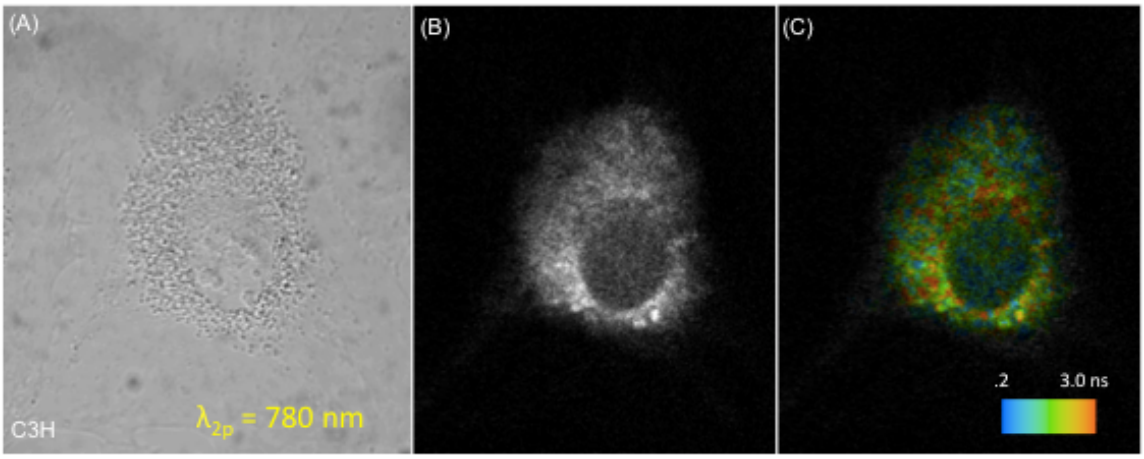

Figure 40: Control DIC and FLIM images for mouse fibroblast cells using 2-photon excitation at 780 nm a) DIC microscopy b) FLIM image without color differentiation of lifetimes c) FLIM image with color coded fluorescence lifetimes

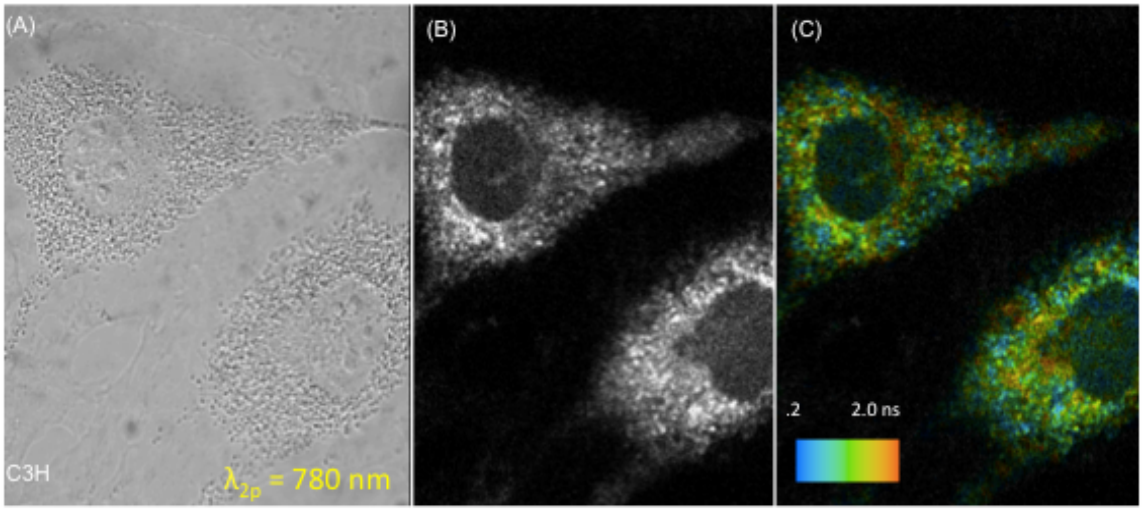

Figure 41: Additional Control DIC and FLIM images for mouse fibroblast cells using 2-photon excitation at 780 nm a) DIC microscopy b) FLIM image without color differentiation of lifetimes c) FLIM image with color coded fluorescence lifetimes

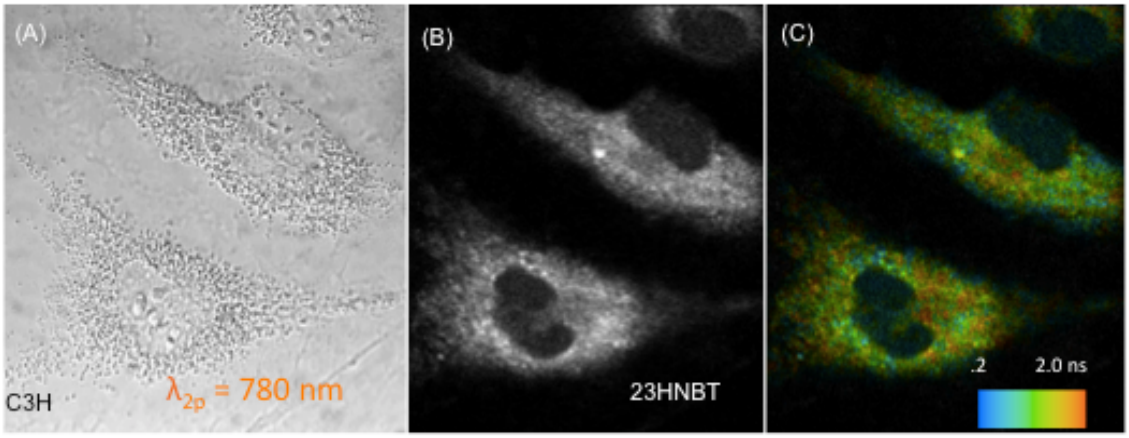

Figure 42: 2-hydroxy-3-naphthoic benzothiazole DIC and FLIM images a) DIC microscopy of mouse fibroblast b) FLIM image 2-photon excitation at 780 nm c) FLIM color coded lifetime image.

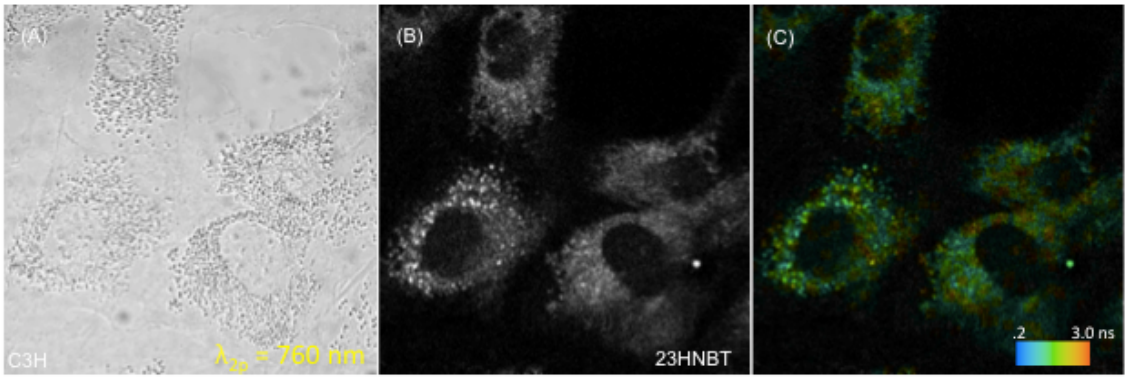

Figure 43: 2-hydroxy-3-naphthoic benzothiazole DIC and FLIM images a) DIC microscopy of mouse fibroblast b) FLIM image 2-photon excitation at 760 nm c) FLIM color coded lifetime image.

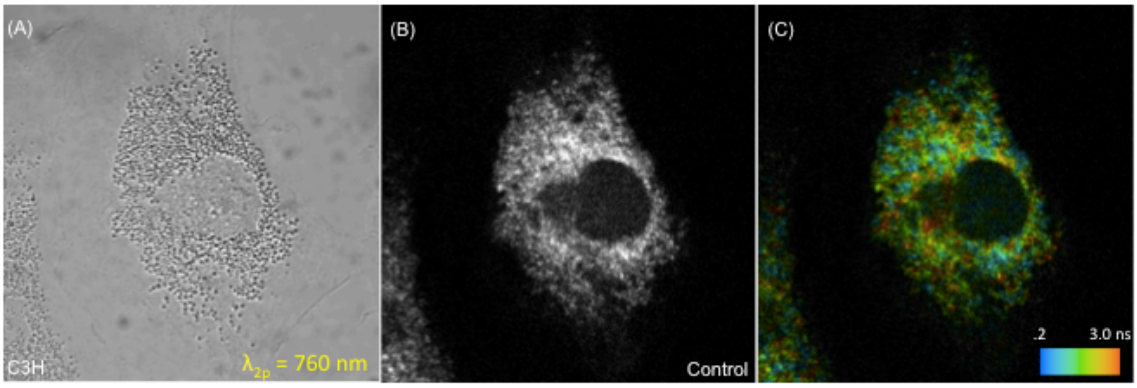

Figure 44: Control DIC and FLIM images for mouse fibroblast cells using 2-photon excitation at 760 nm a) DIC microscopy b) FLIM image without color differentiation of lifetimes c) FLIM image with color coded fluorescence lifetimes

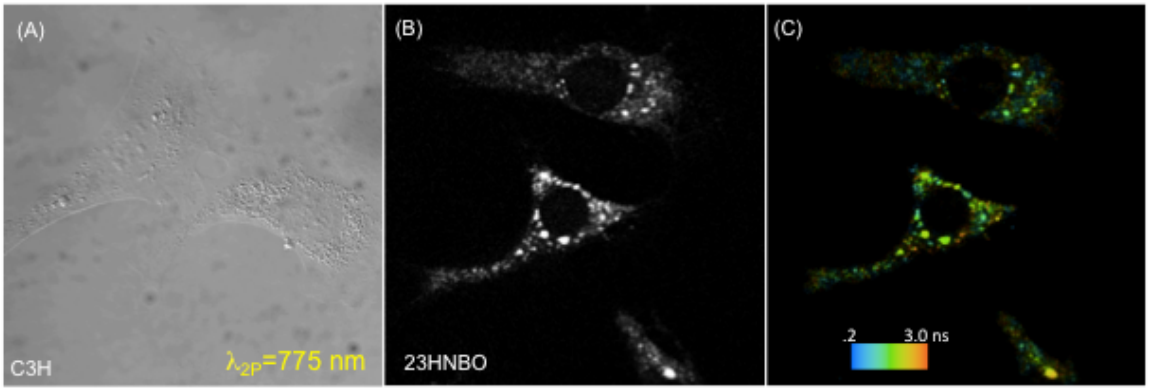

Figure 45: 2-hydroxy-3-naphthoic benzoxazole DIC and FLIM images a) DIC microscopy of mouse fibroblast b) FLIM image 2-photon excitation at 775 nm c) FLIM color coded lifetime image.